Article

Structure

Evidence for a credit-card-swipe mechanism in the human PC floppase ABCB4

Graphical abstract

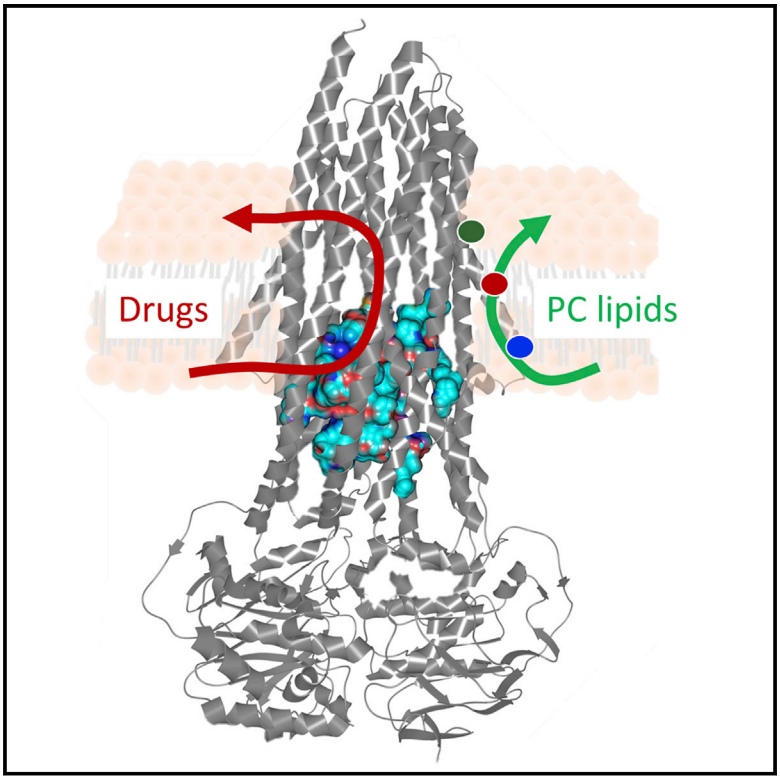

Authors

Martin Prescher, Michele Bonus, Jan Stindt, Verena Keitel-Anselmino, Sander H.J. Smits, Holger Gohlke, Lutz Schmitt

Correspondence

lutz.schmitt@hhu.de

In brief

Prescher et al. demonstrate that ABCB4's second subset of substrates, which overlap with ABCB1's substrates, shows a similar biphasic modulation in both transporters. Amino acid exchanges in TMH1 of ABCB4 prevent stimulation by physiologically relevant phosphatidylcholine lipids. This indicates two distinct and autonomous substrate binding sites in ABCB4.

Highlights

- ABCB4 shows biphasic modulation for drug-like substrates analogous to ABCB1
- This indicates two distinct and autonomous substrate binding sites in ABCB4
- TMH1 is suggested to be involved in phosphatidylcholine lipid flop

Prescher et al., 2021, Structure *29*, 1144–1155
October 7, 2021
https://doi.org/10.1016/j.str.2021.05.013

CellPress

CellPress

Structure

Article

Evidence for a credit-card-swipe mechanism in the human PC floppase ABCB4

Martin Prescher,[1] Michele Bonus,[2] Jan Stindt,[3] Verena Keitel-Anselmino,[3] Sander H.J. Smits,[1,4] Holger Gohlke,[2,5] and Lutz Schmitt[1,*]

[1]Institute of Biochemistry, Heinrich Heine University Düsseldorf, Düsseldorf, Germany
[2]Institute for Pharmaceutical and Medicinal Chemistry, Heinrich Heine University Düsseldorf, Düsseldorf, Germany
[3]Clinic for Gastroenterology, Hepatology and Infectious Diseases University Hospital Düsseldorf, Medical Faculty, Heinrich Heine University Düsseldorf, Düsseldorf, Germany
[4]Center for Structural Studies, Heinrich Heine University Düsseldorf, Universitätsstraße 1, 40225 Düsseldorf, Germany
[5]John von Neumann Institute for Computing (NIC), Jülich Supercomputing Centre (JSC), Institute of Biological Information Processing (IBI-7: Structural Biochemistry) and Institute of Bio- and Geosciences (IBG-4: Bioinformatics), Forschungszentrum Jülich GmbH, 52425 Jülich, Germany
*Correspondence: lutz.schmitt@hhu.de
https://doi.org/10.1016/j.str.2021.05.013

SUMMARY

ABCB4 is described as an ATP-binding cassette (ABC) transporter that primarily transports lipids of the phosphatidylcholine (PC) family but is also capable of translocating a subset of typical multidrug-resistance-associated drugs. The high degree of amino acid identity of 76% for ABCB4 and ABCB1, which is a prototype multidrug-resistance-mediating protein, results in ABCB4's second subset of substrates, which overlap with ABCB1's substrates. This often leads to incomplete annotations of ABCB4, in which it was described as exclusively PC-lipid specific. When the hydrophilic amino acids from ABCB4 are changed to the analogous but hydrophobic ones from ABCB1, the stimulation of ATPase activity by 1,2-dioleoyl-*sn*-glycero-3-phosphocholine, as a prime example of PC lipids, is strongly diminished, whereas the modulation capability of ABCB1 substrates remains unchanged. This indicates two distinct and autonomous substrate binding sites in ABCB4.

INTRODUCTION

ABCB4 is a phosphatidylcholine (PC) floppase localized in the canalicular membrane of hepatocytes (Ruetz and Gros, 1994; Smit et al., 1993; van der Bliek et al., 1987, 1988). Historically, ABCB4 has been called multidrug-resistance (MDR) protein 3 (MDR3) because of its high degree of similarity (76% identity, 86% similarity of the primary structure) to Pgp (MDR1; ABCB1) (Smith et al., 2000). ABCB1, in contrast to ABCB4, is a prototype MDR protein that exports hydrophobic xenobiotics out of the cell (Juliano and Ling, 1976). The small molecular differences between these two ATP-binding cassette (ABC) transporters, however, lead to a large physiological difference. Therefore, it is very likely that the amino acid (aa) differences specifically affect substrate recognition and the translocation mechanism. Interestingly, sequence alignments demonstrate that these differences are distributed over the entire protein, with only a few clusters. One such cluster lies in the N-terminal part and the subsequent transmembrane helix 1 (TMH1).

Molecular differences that influence the substrate spectrum of an ABC transporter are thought to be especially clustered in the transmembrane domain (TMD) since, here, the substrate binding sites are often located, especially in MDR ABC transporters. The substrate binding pocket of ABCB1 is located in the hydrophilic core of the protein approximately at the location of the center of the membrane (Kim and Chen, 2018). It would therefore be easy to assume that aa exchanges that alter the substrate spectrum (or are interchanged between two highly homologous proteins with different substrate spectra) are also present in the region of the central cavity within the TMD. Assuming that a hydrophilic cavity in the center of the protein, as a common substrate binding site comparable to ABCB1 (Alam et al., 2019) or ABCG2 (Manolaridis et al., 2018), also exists in ABCB4, lipid transport, in general, would need to overcome a thermodynamic barrier, if a hydrophobic phospholipid molecule enters an aqueous cavity. The substrate binding site of ABCB4 is not yet described in detail, although recently, the structure of this PC floppase was determined by single-particle cryoelectron microscopy (cryo-EM) (Olsen et al., 2020). Here, ABCB4 was described as an ABC transporter that follows the alternating two-site access model with a substrate binding site analogous to ABCB1 (Hollenstein et al., 2007). However, exact details of how ABCB4 flops PC have remained elusive.

In contrast to the described mechanism for ABCB4 (Olsen et al., 2020), proteins translocating lipids or lipid-like substances, for which this information is present, apparently follow a different

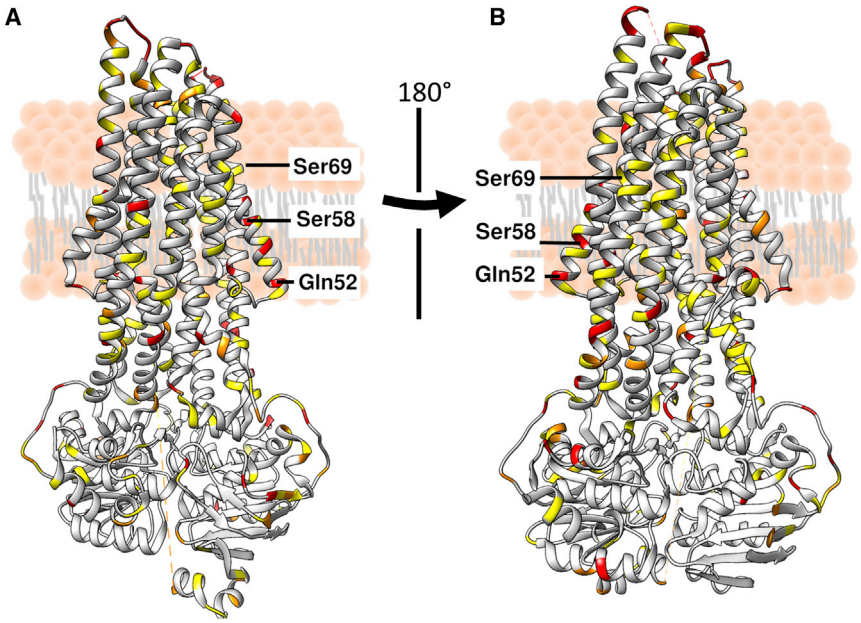

Figure 1. Differences between ABCB1 and ABCB4 on a structural level

(A) Structure of ABCB4 (PDB: 6S7P; Olsen et al., 2020) color-coded according to sequence conservation between ABCB1 and ABCB4 and based on BLOSUM62 scoring (Henikoff and Henikoff, 1992). Yellow corresponds to a moderate change (e.g., R785K, positive BLOSUM62 score), orange to an intermediate change (e.g., V746T, neutral BLOSUM62 score), and red to no conservation (e.g., F760A, negative BLOSUM62 score). Three aas located in TMH1 are highlighted.

(B) View of (A) rotated by 180°.

concept. For lipids or lipid-like substances with a polar head group (lipid head groups or oligosaccharides, respectively) and hydrophobic tails in the form of polyprenyl or fatty acids, the tails do not necessarily have to enter the ABCB4's core. It is sufficient to shield the head group in a translocation cavity at the protein-lipid bilayer interface, while the hydrophobic tail is still embedded in the membrane. ABCB4 following a translocation mechanism based on the alternating two-site access model (like ABCB1 does) would contradict the general features used by other lipid transport (Brunner et al., 2014; Perez et al., 2015; Qian et al., 2017).

For example, PglK is a bacterial transporter that translocates cell-wall precursors employing an outward-only mechanism (Perez et al., 2015). The transporter uses a "substrate-hunting" mechanism with positively charged aas to locally increase the concentration of lipid-linked oligosaccharides prior to transport (Perez et al., 2015, 2019). Increasing the local substrate concentration may facilitate substrate loading into the translocation pathway (Perez et al., 2019). The polyprenyl tail binds to a binding cavity and activates transport but remains embedded in the lipid bilayer (Perez et al., 2015). Even though the translocation process itself requires just one conformation, both states are present and connected through ATP hydrolysis. The inward-facing conformation is probably needed to load the substrate close to a cavity, which is formed only in the outward-facing conformation (Perez et al., 2015).

TMEM16, on the other hand, is a Ca^{2+}-activated lipid scramblase (Brunner et al., 2014). Ca^{2+} binds in the hydrophobic core of the protein at the level of the membrane. Each monomer of the homodimer consists of 10 transmembrane helices. On both sides that face the lipid bilayer, lipid shuffling can occur. This transverse shuffling has no specificity and occurs without the need for ATP hydrolysis. TMEM16 lowers the intrinsic energy barrier associated with lipid flipping by providing a hydrophilic path that is accessible from the membrane and of similar size compared with a polar head group of a phospholipid (Brunner et al., 2014).

Comparatively, ABCB4 and ABCB1 are each coupled, primary active transporters (Al-Shawi et al., 2003; Kluth et al., 2015; Shukla et al., 2017) that require ATP hydrolysis to ensure substrate translocation. Regardless of whether one or two ATPs per transport cycle are required, transport *per se* cannot occur without ATP hydrolysis. In addition to molecular dynamics (MD) simulations and configurational free energy computations, we used this coupling between ATP hydrolysis and substrate transport to gain insights into the transport mechanism of ABCB4.

RESULTS

ABCB1 and ABCB4 share high amino acid sequence identity

ABCB4 and ABCB1 share a high aa sequence identity of 76%. Nevertheless, even if their substrate spectra partially overlap, their physiological roles and evolutionarily optimized substrates, except ATP as a chemical energy source, are remarkably different. Substrate selection is determined by the TMD of ABC transporters. Therefore, first, we scrutinized sequence differences between the two proteins to unravel potential determinants for the functional differences between ABCB4 and ABCB1.

Results of the sequence alignment of ABCB1 and ABCB4 were mapped color-coded onto the structure of ABCB4 (Olsen et al., 2020) to display how aas at the respective positions differ (Figure 1). Yellow corresponds to moderate differences, such as an exchange of an aliphatic side group to another aliphatic side group, and red represents a change of charge or polarity. Note that most of the aa differences are not found in the classical substrate binding pocket of ABC transporters, which is in the hydrophilic core of the protein as identified for the prototype of an MDR exporter, ABCB1 (Alam et al., 2019; Sharom, 2014). There are 55 aa differences within the TMD. Only three aas differ in the putative classical binding pocket in ABCB4 compared with ABCB1: V985, H989, and A990 (Olsen et al., 2020). The other aa exchanges are clustered in other parts of the TMD. Surprisingly, one cluster was located in TMH1, which was not thought to be part of the substrate recognition due to its localization apart from the central cavity and proximity to the lipid bilayer (Figure 1). TMH1 itself harbors 18% of the exchanges (10 of the total 55). Three are particularly

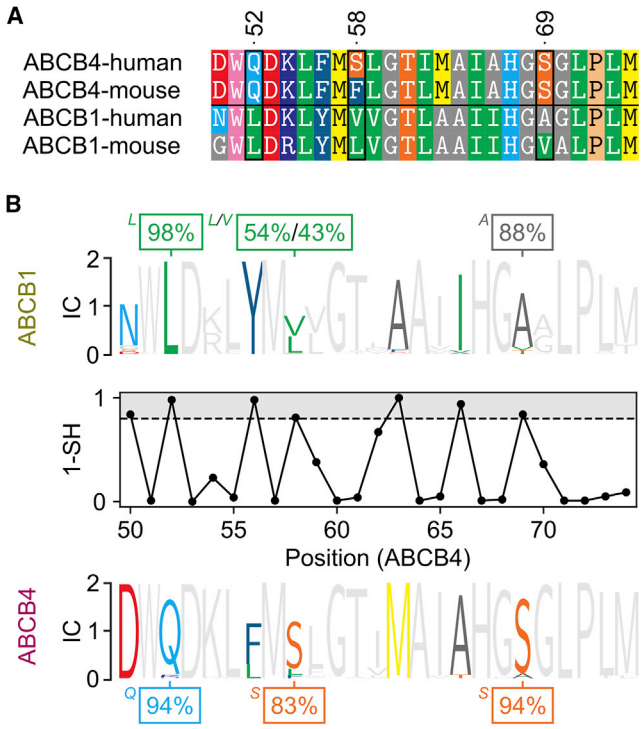

Figure 2. Level of conservation within ABCB4 genes and comparison to ABCB1

(A) Sequence alignment of ABCB4 and ABCB1 from mouse and human in the region of residues 50 to 74 of TMH1.

(B) Conservation of positions 46, 58, and 69 of TMH1 in 65 different species with ABCB1 orthologs (top) and of the equivalent positions 52, 58, and 69 of TMH1 in the same 65 species with ABCB4 orthologs (bottom); percentages indicate the frequency with which the respective aa occurs at the respective position. IC, information content. The analysis of the sequence harmony (SH) is shown between the ABCB4 and the ABCB1 ortholog dataset. Positions above the 1 – SH cutoff of 0.7 (gray-shaded region) indicate specificity-determining residues within ABCB4 and ABCB1. The color scheme is based on the physicochemical properties of the aas: small/hydrophobic (A/G), gray; larger/hydrophobic (V/I/L), green; phenyl/aromatic (F/Y), teal blue; indol/aromatic (W), light pink; nitrogen-containing/polar (Q/N/H), light blue; oxygen-containing/polar (S/T), orange; acidic/negative (D/E), red; basic/positive (K/R), blue; sulfur containing (C/M), yellow; proline (P), light orange.

prominent because of their exchange from nonpolar aas in ABCB1 (L46, V52, A63) to polar ones in ABCB4 (Q52, S58, and S69), as shown for two representative species (human and mouse) (Figure 2A). We analyzed the degree of conservation of these three aas in 65 mammal species that possess both ABCB4 and ABCB1 orthologs (retrieved from https://www.ncbi.nlm.nih.gov, GeneID: 5244 and 5243, respectively). With respect to ABCB4, Q52 was conserved in 61 of 65 cases (94%), S58 in 54/65 (83%), and S69 in 61/65 (94%) (Figure 2B). At equivalent positions in ABCB1, Leu at position 46, Val and Leu at position 52, and Ala at position 63 are the most conserved aas with 98%, 54% (43%), and 88%, respectively (Figure 2B). This indicated a high degree of conservation of the polar aas in ABCB4, especially for positions 52 and 69. In addition, sequence harmony (SH) analysis (Feenstra et al., 2007; Pirovano et al., 2006) between the ABCB4 and the ABCB1 sequences revealed seven specificity-determining residues (SH cutoff = 0.3, Figure 2B) in the TMH1 segment, including all three positions with a hydrophobic-to-polar exchange. This illustrates that these positions particularly contribute to the difference between ABCB1 and ABCB4. As from a thermodynamic point of view, it seems unfavorable that ABCB4 places polar aas to the lipid-facing part of TMH1, these aas may have a functional role. To determine whether the polar residues in TMH1 may be involved in protein-protein interactions, we studied the differences in solvent/membrane accessibility of Q52, S58, and S69 in six homology models of ABCB4 in different conformations (not shown). Regardless of the conformational state of the transporter, the three aas exhibit similar solvent/membrane accessibility, from which it cannot be ruled out that they may be involved in protein-protein interactions.

Evidence for ABCB4-mediated PC flop along TMH1

As a starting point to investigate the lipid transport mechanism of ABCB4, we chose the three aa residues (Q52, S58, and S69) in TMH1. Single, double, and triple mutations were introduced in which the polar aas were replaced by the nonpolar ones of ABCB1 (Figure 3). To allow for a direct comparison of the ATPase measurements between the ABCB4 mutants and the wild type (WT), the data were normalized to the amount of protein and the basal activity, respectively. WT ABCB4 showed 1,2-dioleoyl-*sn*-glycero-3-phosphocholine (DOPC)-dependent stimulation of ATPase activity (black curve in Figure 3A), which reached 500% of the activity observed in the absence of DOPC. In contrast, ABCB4 mutants with mutations L, V, A, LV, and LVA did not show such a degree of stimulation (each mutant versus ABCB4 WT, $p < 0.0001$). Although a residual stimulation was measured for ABCB4 V and ABCB4 LV, ABCB4 A, in particular, was not stimulated above the basal level of ATPase activity (V_{max} values of ABCB4 A versus ABCB4 V and ABCB4 A versus ABCB4 LVA, $p = 0.0001$ and 0.1150, respectively). Notably, this reduction of the DOPC stimulation is reflected by the degree of conservation (Figure 2B). Mutation of the less conserved S58 resulted in a low but still detectable stimulation in the presence of DOPC (190%), whereas the most conserved S69 seems to be crucial for ATPase activity (110%).

To exclude that the loss of stimulation may arise from a partial misfolding of the mutants, we selected two additional compounds that modulate the ATPase activity of ABCB4, digitoxin and verapamil, to analyze the integrity of ABCB4 (Ishigami et al., 2013; Pauli-Magnus et al., 2001; Smith et al., 2000). Digitoxin, a well-known modulator of ABCB1 (Pauli-Magnus et al., 2001), has not been described as a secondary substrate of ABCB4 so far. Interestingly, the well-known bell-shaped dose-response curve was also observed for WT ABCB4 (Figure 3B, black curve). The shape of the curve is probably due to the affinity change of the substrate binding pocket after a conformational change. Here, substrates are bound in the inward-facing conformation with high affinity (high-affinity binding site). ATP is bound, and the outward-facing conformation is adopted. This, in turn, reduces the substrate affinity (low-affinity binding site), and as a result, the substrate is released into the extracellular space. If the concentration of substrate exceeds the affinity of the low-affinity binding site, the outward-facing conformation is arrested, and the transporter can no longer release the substrate. As a result, inhibition of the ATPase activity is observed. An

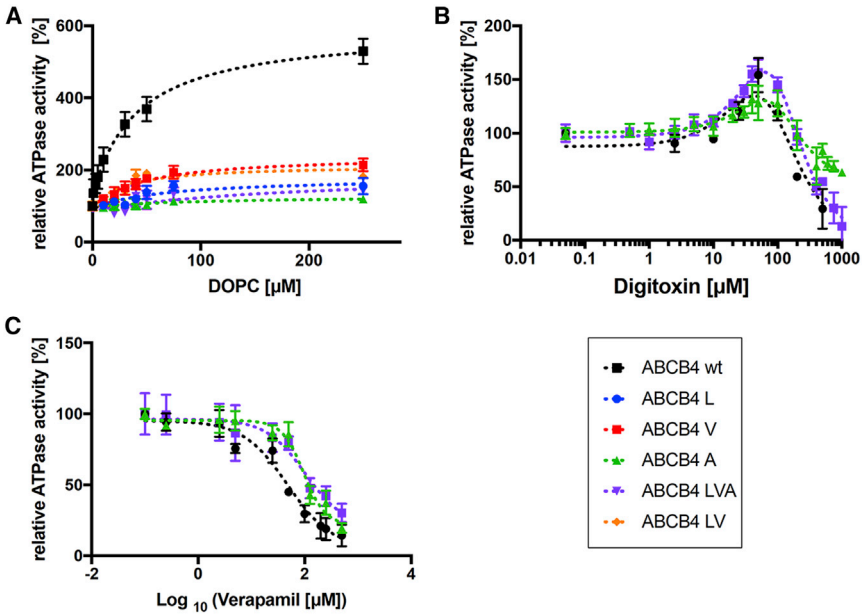

Figure 3. *In vitro* data on the importance of TMH1 to PC-lipid binding

(A) Relative ATPase activity of ABCB4 WT and the mutants Q52L (L), S58V (V), S69A (A), Q52L-S58V (LV), and Q52L-S58V-S69A (LVA) in the presence of increasing concentrations of the phosphatidylcholine lipid 1,2-dioleoyl-*sn*-glycero-3-phosphocholine (DOPC).

(B) Relative ATPase activity of ABCB4 WT and the mutants A and LVA in the presence of increasing concentrations of digitoxin.

(C) Relative ATPase activity of ABCB4 WT and the mutants A and LVA in the presence of increasing concentrations of verapamil. Data shown are the mean ± SEM from $n = 3$ independent experiments.

alternative explanation for this phenomenon was recently provided (Nosol et al., 2020). In this study, cryo-EM structures of inhibitor-bound ABCB1 revealed that inhibitors may bind in pairs, with one entity occupying the classical drug-binding site and the other occupying an "access tunnel" located along the path to the drug binding site. This would arrest the transporter and decrease ATPase activity. Most importantly, WT and all mutants of ABCB4 displayed similar dose-response curves in the presence of increasing concentrations of digitoxin (Figure 3B). In addition, we analyzed the ATPase activity of WT ABCB4 and the mutants in the presence of verapamil (Figure 3C), a well-known inhibitor of ABCB1 (Smith et al., 2000) and ABCB4 (Duan et al., 2004; Smith et al., 2000). Again, no significant differences between the inhibition of ATPase activity of the WT and the mutants were observed (ABCB4 WT versus ABCB4 A and ABCB4 WT versus ABCB4 LVA, p = 0.562 and 0.761, respectively). Importantly, we observe quantitative or nearly quantitative inhibition for WT and all mutants for all compounds, suggesting that the model of Nosol et al. (2020) likely does not apply here.

If we modified the substrate binding pocket in the mutants, substrate-dependent ATPase activity should be changed or even become independent of substrate concentration. This was not the case for the modulator digitoxin and the inhibitor verapamil, demonstrating that the architecture of the digitoxin and verapamil binding sites is not modified in the mutants and that the mutants remain functional. By contrast, DOPC-dependent stimulation of ATPase activity changed in ABCB4 mutants. These results demonstrate that the drug and lipid binding sites are different, i.e., classical ABCB1 substrates are recognized different from PC lipids by ABCB4, although both compound classes have hydrophobicity in common.

Cavities within the proteins differ between ABCB1 and ABCB4

The structural comparison of ABCB1 and ABCB4 reveals that the cavity of ABCB4 has a smaller volume and is somewhat globular (Figure 4A), whereas that of ABCB1 is more pore-like (Figure 4B). Thus, in the case of ABCB1, the cavity spans the entire membrane, but it covers only the inner membrane leaflet in the case of ABCB4. However, note that the structure of ABCB4 represents an outward-facing but closed conformation (Olsen et al., 2020). No similar conformation has been described for ABCB1. The most similar conformation of ABCB1 is outward facing and open (Kim and Chen, 2018) (Figure 4B), which differs by 1 Å C_α atom root-mean-square deviation from that of ABCB4. Even though the different cavity sizes may originate from different conformations, the 40% larger cavity in ABCB1 is somewhat surprising, given such similar structures, and goes in hand with the more promiscuous substrate spectrum.

ABCB4 restricts lipid access

To determine whether and to what extent ABCB1 and ABCB4 can take up and bind DOPC lipids in their substrate cavity, we conducted five independent all-atom MD simulations of 200 ns each of each transporter, starting from the inward-facing conformation embedded in an explicit DOPC membrane.

For the alternating two-site access model to occur, in this conformation, a potential substrate in the inner leaflet, must first traverse one of the two entry gates (front gate, TMH3/4/6; rear gate, TMH9/10/12) to enter the hydrophobic substrate cavity. Therefore, we first determined differences in the accessibility of the substrate cavities of ABCB1 and ABCB4. In all MD simulations of ABCB1, both entry gates were wide open on average (Figure 5A); by contrast, in all MD simulations of ABCB4, at least one of the entry gates was constricted or completely closed (Figure 5B). We furthermore counted the number of bound lipids for each simulation snapshot. ABCB1 accommodated, at least partially, up to four lipids in its substrate cavity (Figure 5C, left), but ABCB4 never took up more than one lipid (Figure 5C, right). Finally, we computed the average number of snapshots in which one lipid was bound. In 64.8% ± 9.4% (mean ± SEM) of all snapshots of an ABCB1 simulation, at least one DOPC molecule crossed the boundary to the substrate cavity. By contrast, this applies to only 18.8% ± 12.5% of all snapshots of an ABCB4 simulation. Together, these results suggest that in ABCB4, unlike

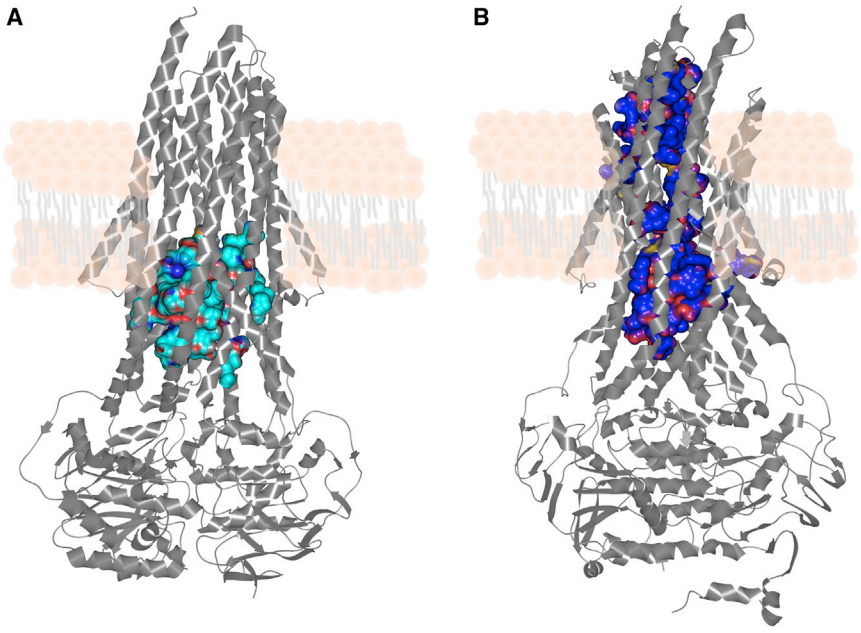

Figure 4. Cavities of ABCB1 and ABCB4

(A) Structure of ABCB4 (PDB: 6S7P; Olsen et al., 2020) highlighting the cavity (solid) with a volume of 3,756 Å^3 in an ATP-bound, closed conformation.

(B) Structure of ABCB1 (PDB: 6C0V; Kim and Chen, 2018) highlighting the cavity (solid) with a volume of 5,325 Å^3 in an ATP-bound outward-facing conformation. Both computations were performed with Caver (Chovancova et al., 2012), using a probe size of 1.4 Å.

in ABCB1, lipid access to the substrate cavity is markedly restricted.

Q52 in ABCB4 may pre-organize PC lipids near TMH1

Next, using the same set of MD simulations, we probed for evidence of phospholipid pre-organization at the base of TMH1 in ABCB4 compared with the base of TMH1 in ABCB1. To do so, we computed the residence probability of DOPC molecules in the lower leaflet. The residence probability was higher near TMH1 than near TMH7 in both simulation systems (Figure 6A); TMH7 is the structural equivalent of TMH1 in the other pseudo-half of the transporter. The magnitude of the residence probability of DOPC molecules near TMH1 differed little overall between ABCB1 and ABCB4 (Figure 6B), except for the high probability close to the highly conserved Q52 in ABCB4. In ABCB1, a higher residence probability is caused by R144 of TMH2 (Figure 6B). This result suggests that the residues, located in the head-group region of the membrane, help in pre-organizing DOPC molecules near TMH1 of ABCB4.

Configurational free energy computations of DOPC flip-flop and ABCB4-mediated DOPC translocation

Using steered MD simulations, umbrella sampling (Kästner, 2011), and potential of mean force (PMF) computations applying the weighted histogram analysis method (Kumar et al., 1992; Souaille and Roux, 2001), we next studied the differences in the configurational free energy between ABCB4-mediated DOPC translocation and DOPC flip-flop across a DOPC membrane. In total, we sampled four pathways, along each of which the PMF was calculated: (1) DOPC flip-flop from the inner to the outer membrane leaflet in a pure DOPC membrane, (2) DOPC translocation along TMH1 of inward-facing ABCB4 (Figures 7A and 7B), (3) DOPC translocation along TMH7 of inward-facing ABCB4, and (4) DOPC translocation along TMH1 of ABCB4 in the outward-closed conformation.

We calculated the free energy barrier for an unassisted DOPC flip-flop in a pure DOPC membrane as 20.42 ± 0.48 kcal mol^{-1} (Figure 7C, top), which is in good agreement with the experimentally determined flip-flop rate for spin-labeled PC (Kornberg and McConnell, 1971) (0.04–0.07 h^{-1}, corresponding to 24.3–24.6 kcal mol^{-1} according to the Eyring equation) and the calculated free energy barrier for DOPC flip-flop in a pure DOPC membrane (Sapay et al., 2010; Tieleman and Marrink, 2006) (~22.5 kcal mol^{-1}). This free energy barrier decreased by 6.8 kcal mol^{-1} when DOPC was translocated along TMH1 of ABCB4 (Figure 7C, top). Notably, this difference corresponds to the gain in free energy due to ATP hydrolysis, which is 7.3 kcal mol^{-1} under physiological conditions (Rosing and Slater, 1972). In addition, the rate difference between spontaneous (average from Kornberg and McConnell, 1971) and ABCB4-assisted flip-flop (this study, cf. STAR methods data evaluation) relates to a decrease in the free energy barrier of 5.23 ± 0.20 kcal mol^{-1}, close to our computed value. Among the hydrophilic residues along the transmembrane segment of TMH1, S69 stood out, since the most prominent differences in the free energy profile are found in its vicinity (Figure 7C, top). By contrast, no major differences were detected in the region of S58. Nevertheless, since the S58V mutant displayed a significantly reduced DOPC-stimulated ATPase activity (Figure 3A), we speculate that S58 controls the correct positioning of DOPC during translocation and that ATPase activity is stimulated only when the lipid reaches the vicinity of S69. We further found evidence that the observed decrease in the free energy barrier is specific for translocation along TMH1, since translocation along TMH7 did not result in a barrier decrease (Figure 7C, middle). TMH7 does not contain polar aas pointing to the membrane interface.

Moreover, a decrease in the free energy barrier is found only when DOPC is translocated along TMH1 of the inward-facing conformation and not the outward-closed conformation (Olsen et al., 2020) (Figure 7C, middle). An overlay of the free energy profiles for the two conformations reveals that the first half of the translocation pathway is more favorable in the outward-closed conformation, but the second half is more favorable in the inward-facing conformation (Figure 7C, bottom). This comparison suggests that binding,

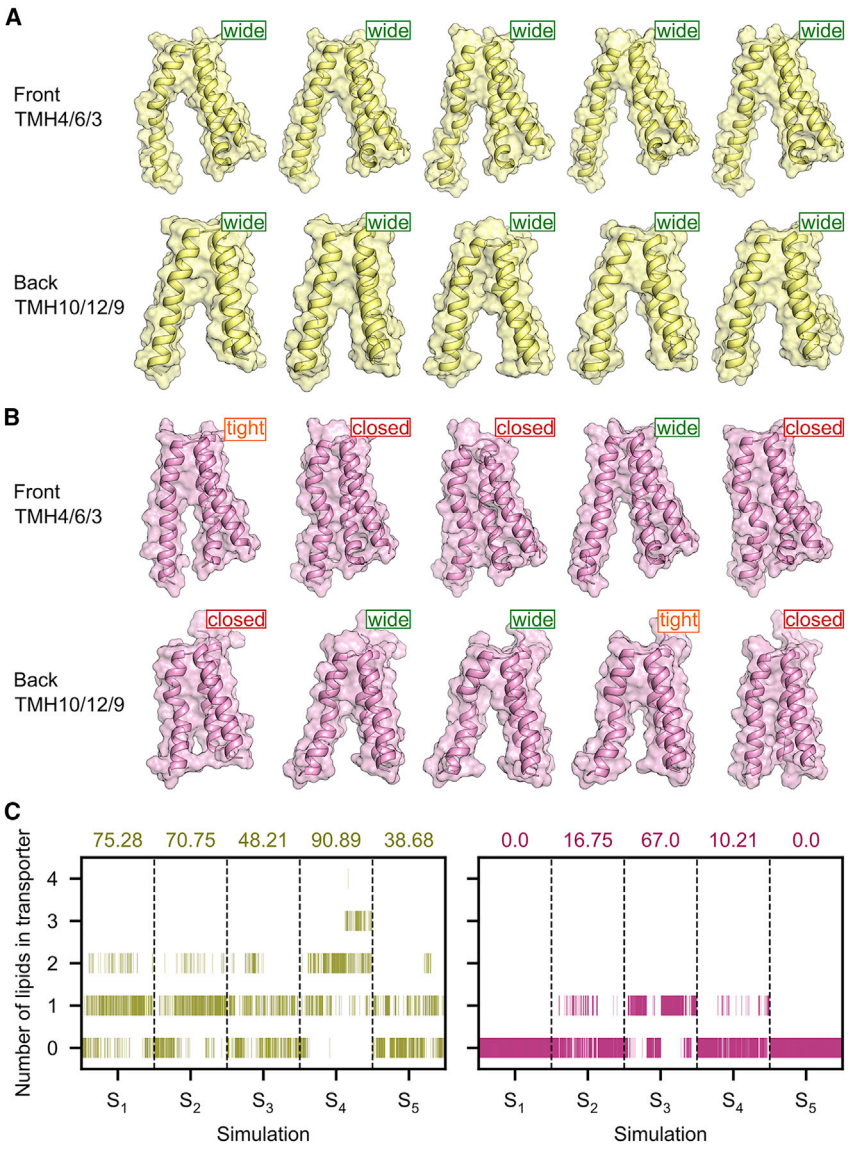

Figure 5. Lipid binding to the substrate cavities of ABCB1 and ABCB4

(A) Closest-to-average structure of the front gate (formed by TMH4, TMH6, and TMH3) and rear gate (formed by TMH10, TMH12, and TMH9) to the substrate cavity of ABCB1, extracted from five independent MD simulations of inward-facing ABCB1 embedded in a DOPC membrane.

(B) Closest-to-average structure of the front gate (formed by TMH4, TMH6, and TMH3) and rear gate (formed by TMH10, TMH12, and TMH9) to the putative substrate cavity of ABCB4, extracted from five independent MD simulations of inward-facing ABCB4 embedded in a DOPC membrane.

(C) Time course of DOPC binding into the substrate cavity of ABCB1 (left, golden) and ABCB4 (right, purple), determined from five independent MD simulations (S_1–S_5) of each system. The percentage of snapshots in which at least one DOPC molecule was bound to the substrate cavity is given above the plot for each simulation. A DOPC molecule is classified as bound if its phosphate atom lies within the bounding box around the position of the Cα atoms of TMH3, TMH4, TMH9, and TMH10 and is located between the innermost Cα atoms of the helix pairs TMH3/TMH4 and TMH9/TMH10.

positioning, and initial translocation of the hydrophilic lipid head group into the membrane occur in the outward-facing or outward-closed conformation. By contrast, the energetically most demanding step—the transfer of the head group across the center of the membrane—occurs in the inward-facing conformation. These findings can rationalize the need for ATP hydrolysis-mediated conformational changes in ABCB4 during translocation.

Stability calculations for the ABCB4 to ABCB1 triple mutant

Previously, an ABCB4 triple mutant (V985M + H989Q + A990V; Olsen et al., 2020) was generated in which all residues in the ABCB4 cavity, whose equivalents in ABCB1 are involved in the binding of the inhibitor zosuquidar, were converted to the corresponding ABCB1 residues. The triple mutant revealed a pronounced functional impairment, which may indicate that these residues are directly involved in DOPC transport. Alternatively, these mutations may have an impact on conformational changes in ABCB4 and, hence, DOPC transport indirectly. To assess the potential impact of these mutations on the stability of the outward-closed (PDB: 6S7P; Olsen et al., 2020) and inward-open (comparative model from PDB: 4M1M; Li et al., 2014) conformations of ABCB4, we computed the change in single-point free energy between the triple mutant and the WT ABCB4. Irrespective of the calculation settings, the triple mutant is thermodynamically more stable than the WT ($\Delta\Delta G$ = −71.73 to −2.55 kcal mol^{-1}), and this effect is consistently more pronounced for the outward-closed conformation (Figure 8). These data lead to the hypothesis that the triple mutant may lock the conformational cycle of ABCB4 in the outward-closed conformation, which could provide an alternative explanation for the observed functional impairment in addition to a direct involvement in DOPC transport.

DISCUSSION

Despite their high sequence identity of 76%, ABCB1 and ABCB4 fulfill different physiological roles. ABCB1 is a prototype drug exporter, whereas ABCB4 flops PC lipids in the canalicular membrane of the liver. Here, we provide evidence from the *in vitro* characterization of WT ABCB4 and mutants, as well as molecular simulations, that PC flop can occur along TMH1 of ABCB4 due to the presence of polar aas located within the lower leaflet along the translocation pathway.

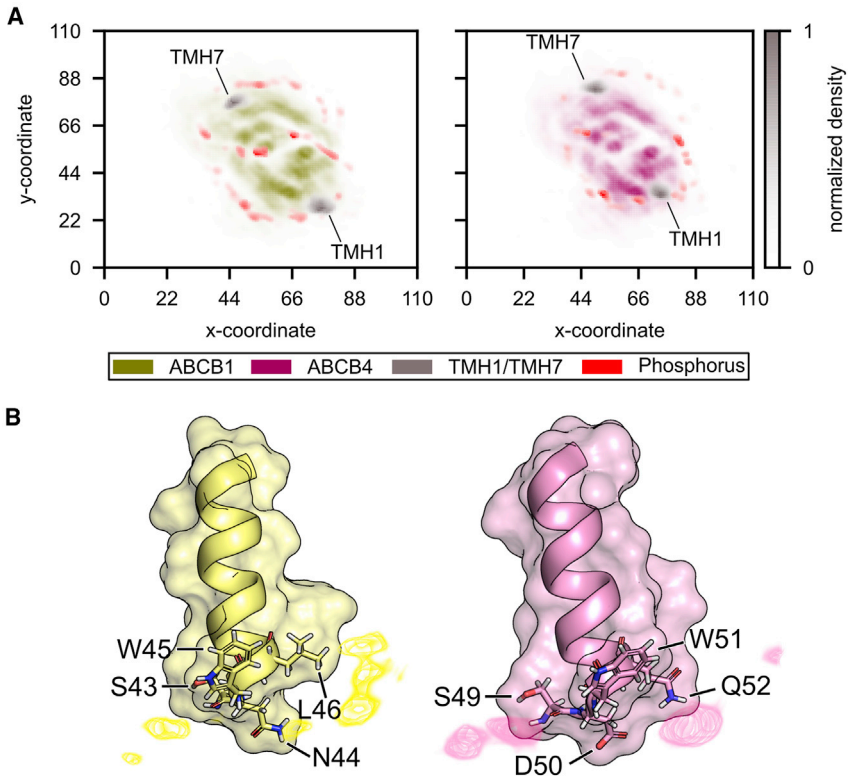

Figure 6. Comparison of the residence probability of DOPC in simulation systems containing ABCB1 (yellow) and ABCB4 (purple)

(A) The z-axis-averaged residence probabilities of the backbone atoms of ABCB1 (left, yellow) and ABCB4 (right, purple), Cα atoms of the first helical turn of TMH1 and TMH7 (gray), and phosphorus atoms of the DOPC molecules in the lower leaflet of the membrane (red). The values for each grid point were normalized to values between 0 and 1 for each grid type individually and are encoded through the opacity of the respective color (see color scale on the right).

(B) Visualization of regions with high residence probabilities of DOPC near the N terminus of TMH1 in ABCB1 (yellow, left) and ABCB4 (purple, right). The volumes represented as wireframe enclose regions of high probability; the same contour levels were used.

ABCB4 and ABCB1: Highly similar sequence, but different physiological roles

Due to translocation efficiencies, ABCB1 and ABCB4 most likely do not interfere with each other *in vivo*. Each protein translocates only its substrates despite a partly overlapping substrate spectrum under *in vitro* circumstances (Smith et al., 2000; van Helvoort et al., 1996). However, some substances are exclusive for each of the ABC transporters, pointing also to significant differences in their translocation mechanisms (Smith et al., 2000; van Helvoort et al., 1996). Thus, ABCB4 may have developed a distinct mechanism for the translocation of PC lipids during evolution, although the primordial mechanism typical for ABCB1, in which the central cavity has a dominant role for substrate translocation, is still intact. The primordial mechanism might be in the state of evolutionary regression in ABCB4, which could explain the narrower substrate spectrum and reduced translocation efficiency for ABCB1 substrates. The cavity in ABCB4 is 40% smaller than in ABCB1 (Figure 4) and does not span the complete length of the membrane, at least in the determined conformation. By contrast, the pore-like cavity in ABCB1 reaches the extracellular space. The differences are remarkable, given that both structures are very similar, and concordant with a more specific substrate spectrum of ABCB4. Furthermore, unbiased MD simulations started from inward-facing conformations showed open entry gates on average for ABCB1 (Figure 5A) but at least one of the entry gates constricted or completely closed in ABCB4 (Figure 5B), suggesting that the substrate uptake through a lateral gate is different and less pronounced in ABCB4.

Still, ABCB4 might contain a drug binding site and utilize the typical ABCB1 export mechanism whenever the apparent drug concentration exceeds a certain threshold and the shape of the drug is compatible with the shape of the central cavity. Both necessities are most likely not fulfilled under physiological conditions but can be achieved in *in vitro* circumstances. This hypothesis is supported by the observation that ABCB4 shows the same bell-shaped ATPase activation pattern as ABCB1 *in vitro* in the case of digitoxin (Figure 3B). It has been shown in whole-cell experiments and cell-culture-based assays that ABCB4 is capable of exporting classical ABCB1 substrates (Duan et al., 2004). However, this translocation is significantly slower than the transport rates of ABCB1. Duan et al. demonstrated that ABCB4 siRNA-treated cell lines showed minor reductions in paclitaxel resistance, consistent with the observation of lower transport rates of paclitaxel by ABCB4 than ABCB1 (Duan et al., 2004; Smith et al., 2000).

In addition to the translocation pathway of an ABC transporter substrate, the target compartment of a substrate after translocation is also an important point of discussion. This is true for all transporters, but especially for MDR-facilitating transporters such as ABCB1, ABCC1, and ABCG2, the substrates of which are predominantly hydrophobic (Kroll et al., 2020). Regardless of the mechanism by which the substrates of these transporters are translocated, we consider the extracellular compartment an unlikely target. When a hydrophobic substrate is moved from the outward-facing transporter to the aqueous extracellular space, it would need to overcome an additional free energy barrier, the height of which is dependent on the hydrophobicity of the substrate. However, if the substrate were released directly into the outer membrane leaflet, the energetic costs of transferring the hydrophobic substrate into the aqueous medium would be avoided. PC lipids translocated by ABCB4 would end up in the outer membrane leaflet. Transfer of a lipid from the outer leaflet into the extracellular space is associated with an energy barrier similar to that of its unassisted transversal flip-flop (Tieleman and Marrink, 2006). Accordingly, it is reasonable to assume that the transfer of DOPC from an outward-facing cavity into

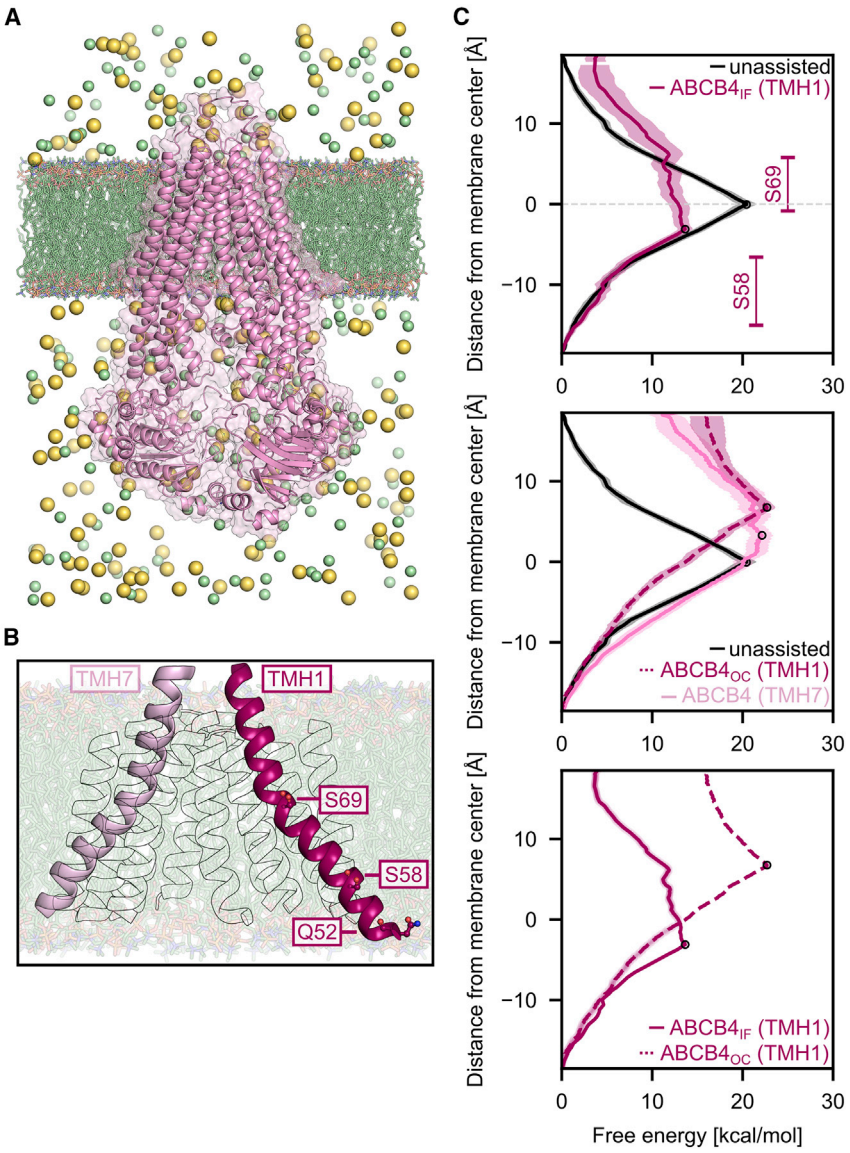

Figure 7. Configurational free energy calculations of DOPC flip-flop and ABCB4-mediated DOPC translocation

(A) Representation of the complete simulation system. ABCB4 (purple) is shown in cartoon and surface representation. The DOPC membrane (green) is shown as sticks. Na^+ and Cl^- ions are depicted as yellow and light green spheres, respectively.

(B) Transmembrane region of ABCB4. TMH1 and TMH7 are highlighted in dark purple and pink, respectively. Hydrophilic residues in TMH1 that have been exchanged in mutation experiments are highlighted.

(C) Free energy profiles of DOPC flip-flop in a DOPC membrane (black), DOPC translocation along TMH1 (dark purple), and DOPC translocation along TMH7 (pink). The free energy profile of DOPC translocation along TMH1 of outward-closed (OC) ABCB4 is indicated with a dashed line. Uncertainties are expressed as standard deviation and depicted as transparent areas (upper and middle plots). The locations of the side-chain oxygen atoms of S58 and S69 during the simulation are displayed with 2 SD (upper plot).

the extracellular space is associated with a similarly high barrier. Thus, the process of releasing DOPC into the extracellular space in the absence of a specific lipid acceptor is likely not biologically relevant.

Evidence for TMH1 as an anchor point for lipid translocation

Most of the aa differences between ABCB1 and ABCB4 occur in protein regions facing the membrane. This provided a hypothesis for how ABCB4 can transport PC lipids, whereas ABCB1 cannot, based on general features described for other lipid transport systems (Brunner et al., 2014; Perez et al., 2015). One such region in TMH1, located primarily in the lower leaflet, is crucially different in ABCB4 and ABCB1 (Figure 1). Therefore, we asked if this area is involved in substrate-protein interactions by introducing mutations there. Substituting three polar aas found in ABCB4 alone or in combinations with nonpolar ones located in ABCB1 at these positions reduced relative ATPase activity in a site-specific manner (Figure 3A). Substitutions of residues 52 (located in the head-group region) and 69 (located close to the membrane center) decreased relative ATPase activity the most. Hence, having polar aas on the outside of TMH1 allows ABCB4 to translocate PC lipids, but substitutions with nonpolar ones diminish or abrogate it.

These data on inhibited ATPase activity, together with the data from the MD simulations and configurational free energy computations, indicate that PC lipids are shifted along TMH1 from the inner to the outer leaflet, forming favorable interactions between the polar head group and the polar residues, but without forcing the hydrophobic tail into a water-filled cavity in the protein interior, as would be the case in the typical ABCB1 export mechanism. Initially, Q52 may pre-organize PC lipids near the N terminus of TMH1 as indicated by a higher residence probability than for TMH7 of ABCB4 or TMH1 of ABCB1 (Figure 6), which may explain its relevance in the mutation studies. Upon moving to the membrane center during the flop, the polar head group needs to strip off at least part of its water shell, which is unfavorable. The polar residues on TMH1 along the translocation pathway can act as substitute interaction partners, as indicated by a free energy barrier 6.8 kcal mol^{-1} lower than that for an unassisted PC flip-flop (Figure 7C). Based on the rates obtained by Kornberg for spontaneous DOPC flip-flop (Kornberg and McConnell, 1971) and the rates for ABCB4-assisted DOPC translocation determined in this study, the expected reduction in barrier height determined by the Eyring equation would be 5.23 ± 0.2 kcal mol^{-1}, which is in close agreement with our

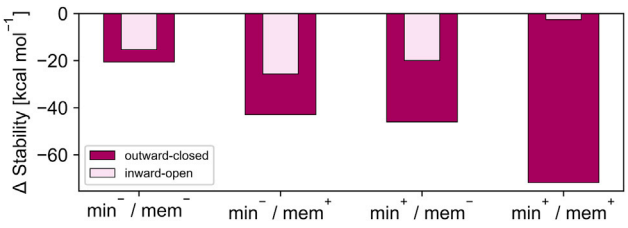

Figure 8. Single-point free energy calculations for the outward-closed and inward-open ABCB4-to-ABCB1 triple mutant

For the outward-closed conformation PDB: 6S7P (Olsen et al., 2020) (purple) and for the inward-open conformation a comparative model from PDB: 4M1M (Li et al., 2014) (pink) of the ABCB4-to-ABCB1 triple mutant (V985M + H989Q + A990V) were used. Protein structures were taken as either deposited (min$^-$) or pre-minimized (min$^+$), and stability calculations were performed either without (mem$^-$) or with (mem$^+$) an implicit membrane.

calculations. Note, however, that experimentally determined rates for spontaneous lipid flip-flop vary considerably depending on the experimental setup (Epand and Ruysschaert, 2017). The barrier decrease is associated with the region of S69 located in the membrane center, concordant with the aa role in the mutation studies. Expectedly, no such decrease was observed along TMH7, which bears no membrane-facing polar residues (Figure 7C). Beyond the membrane center, the configurational free energy decreases such that the PC lipid would spontaneously complete the flop. The driving force is the gain of the water shell around the polar head group. In the outer head-group region, the configurational free energy of the PC lipid at TMH1 is ~4 kcal mol^{-1} higher than at the inner region (Figure 7C). This is likely caused by a missing analog of Q52 in the outer head-group region and may explain why ABCB4 acts as a floppase but not a flippase. The rise in configurational free energy from the inner head-group region to the membrane center is higher by up to ~4 kcal mol^{-1} in the case of the inward-facing ABCB4 conformation compared with the outward-closed one (Figure 7C). Beyond the membrane center, the configurational free energy for PC lipid flop along the inward-facing conformation is ~10 kcal mol^{-1} lower. This result may explain why ATP hydrolysis and associated conformational changes in ABCB4 are required for a complete PC lipid flop: the PC lipid translocation starts in the outward-closed conformation with ATP bound, which upon hydrolysis drives the conversion to the inward-facing state, allowing the completion of the translocation. However, without detailed structural information of the state just before ATP hydrolysis, it is not possible to derive an exact model that can explain how ATPase activity is stimulated on a molecular level and how TMH1 communicates with the nucleotide binding domain (NBD) (Figure 9). As for ABCB1, there is evidence that the process of substrate translocation itself does not require ATP hydrolysis. Instead, ATP hydrolysis serves to restore the ground state and, thus, to complete one transport cycle (Szöllősi et al., 2020). If such a mechanism is also operational in ABCB4, translocation and re-setting will occur at the same stage. One also has to stress that one cannot distinguish both scenarios based on our results. The mutations of the polar residues at TMH1 abolished the DOPC-stimulated ATPase activity, but neither the basal activity nor the modulation by digitoxin or verapamil. Together with our computational results, these data provide indirect evidence that PC lipids act as substrates of ABCB4 even in the detergent-purified state. In addition, no differences in ATPase activity of either the WT protein or the mutants were observed in the presence of the inhibitor (verapamil) or the modulator (digitoxin). Although the ATPase activity is an indirect readout for transport, this clearly indicates the presence of two distinct translocation pathways in ABCB4, one used for ABCB1 substrates and one for PC lipids.

Here, we have provided strong evidence for a credit-card-like swipe transport mechanism for PC lipids in ABCB4. The conclusions are based on loss-of-function mutants, i.e., mutations that abolished stimulation of ATPase activity. The final goal would be to complete our data with gain-in-function mutants in ABCB1, in which the equivalent sets of mutations in TMH1 of ABCB1 would convert ABCB1 into a PC lipid floppase. Although this is beyond the scope of this study, which provided the foundation for a working mechanism of ABCB4 as a PC floppase, it will be required to fully understand the similarities and differences of ABCB1 and ABCB4 on the molecular level.

Relation to other systems translocating lipids or lipid-like structures

Families of other proteins interacting with and translocating lipids or lipid-like structures face the same challenge of pulling an amphipathic substrate out of the membrane into a potentially hydrophilic cavity. PglK is a bacterial transporter that translocates cell-wall precursors with an outward-only mechanism (Perez et al., 2015). Here the pyrophosphate oligosaccharide-linked head group interacts with positive charges of PglK. The polyprenyl tail binds initially to the protein facing the lipid bilayer and activates transport, but remains embedded in the lipid bilayer (Perez et al., 2015). Even though the translocation process itself needs only one conformation, both states can be achieved through ATP hydrolysis. The inward-facing conformation is probably needed to load the substrate in close proximity to a cavity that is formed only in the outward-facing conformation. Therefore, the inward-facing conformation exhibits a stage where loading, but not translocation, takes place (Perez et al., 2015). The decrease in the configurational free energy for the shift of a PC lipid along TMH1 was observed only with the inward-facing conformation of ABCB4. We speculate then that ABCB4, as shown for PglK, is a lipid transporter that needs only one conformation for lipid translocation, and the other conformation is required for loading purposes (Perez et al., 2015).

The TMEM16 scramblase, on the other hand, is a Ca^{2+}-activated lipid scramblase (Brunner et al., 2014). Ca^{2+} binds in the hydrophobic core of the protein at the height of the membrane. Each monomer of the functional homodimeric protein consists of 10 transmembrane helices. Lipid shuffling can take place on both sides that are facing the lipid. This transverse shuffling has no specificity and, therefore, all phospholipids are shuffled equally well without the need of ATP hydrolysis (Brunner et al., 2014).

ABCB4/ABCB1 hybrids revealed a crucial role for the extracellular loops and three residues in the protein core (Olsen et al., 2020). The three aas V985, H989, and A990 in the protein's interior may be required for substrate translocation or are simply part

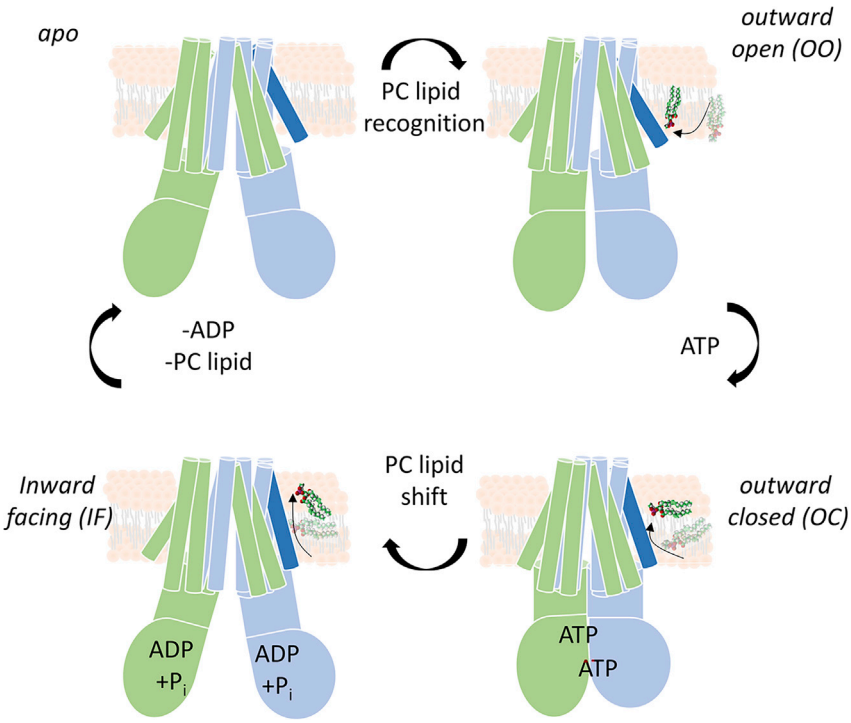

Figure 9. Suggested transport mechanism of ABCB4 derived from configurational free energy landscapes

The outward-open structure may be needed for substrate loading to TMH1 (dark blue). A transition to the outward-closed structure may be initiated by substrate recognition and ATP binding and is suggested to facilitate the first half of the lipid translocation. ATP hydrolyzation resets the transporter to the inward-facing structure, which is suggested to facilitate the second half of lipid translocation.

of the substrate binding site following the alternating two-site access model known from ABCB1 (Olsen et al., 2020). However, they may also mediate a signal to the NBDs only after substrate recognition at the TMH1 in order to dimerize the NBDs and change conformation. This would therefore influence the protein's activity but not specifically interrupt protein substrate interactions. Moreover, our single-point free energy calculations suggest that the V985M + H989Q + A990V triple mutant may overstabilize the outward-closed conformation, thus interrupting the conformational cycle of ABCB4. In addition, the ATPase measurements we performed provided insights into the substrate protein interaction on a minute timescale, whereas the translocation assay from Olsen et al. (2020) required 24 h.

In summary, we provided evidence that PC flop can occur along TMH1 of ABCB4 due to the presence of polar aas located within the lower leaflet along the translocation pathway. These results suggest, together with findings on other lipid transporting systems, that proteins translocating lipids commonly do this by interacting with them in membrane proximity rather than pulling a lipid into the protein's interior. For ABCB4, a translocation pathway along TMH1 would reduce the thermodynamic penalty for pulling a lipid out of its native bilayer and placing it into a water-filled cavity.

STAR★METHODS

Detailed methods are provided in the online version of this paper and include the following:

- KEY RESOURCE TABLE
- RESOURCE AVAILABILITY
  - Lead contact
  - Materials availability
  - Data and code availability
- EXPERIMENTAL MODEL AND SUBJECT DETAILS
- METHOD DETAILS
  - *In vitro* characterization of ABCB4 and its mutants
  - Molecular modeling and simulations
- QUANTIFICATION AND STATISTICAL ANALYSIS
  - ABCB4 and ABCB1 orthologs
  - Calculation of the ATPase activity

SUPPLEMENTAL INFORMATION

Supplemental information can be found online at https://doi.org/10.1016/j.str.2021.05.013.

ACKNOWLEDGMENTS

We thank all the members of the Institute of Biochemistry for fruitful discussions. This work was supported by the Deutsche Forschungsgemeinschaft (Funder ID 10.13039/501100001659, CRC 974 project B03 to L.S.; Funder ID GO 1367/2-2, FOR 2518 project TP7 to H.G.). The Center for Structural Studies is funded by the DFG through grant 417919780 to S.S.

AUTHOR CONTRIBUTIONS

Conceptualization, H.G., S.H.J.S., V.K.-A., and L.S.; methodology, M.P., M.B., H.G., S.H.J.S., and L.S.; software, M.B. and H.G.; validation, M.P., M.B., H.G., S.H.J.S., V.K.-A., J.S., and L.S.; formal analysis, M.P., M.B., H.G., and L.S.; investigation, M.P. and M.B.; resources, H.G. and L.S.; writing – original draft, M.P. and M.B.; writing – review & editing, M.P., M.B., H.G., S.H.J.S., V.K.-A., J.S., and L.S.; visualization, M.P. and M.B.; supervision, V.K.-A., H.G., and L.S.; funding acquisition, H.G., V.K.-A., and L.S.;

DECLARATION OF INTERESTS

The authors declare that they have no competing interests.

Received: February 8, 2021
Revised: April 27, 2021
Accepted: May 17, 2021
Published: June 8, 2021

REFERENCES

Al-Shawi, M.K., Polar, M.K., Omote, H., and Figler, R.A. (2003). Transition state analysis of the coupling of drug transport to ATP hydrolysis by P-glycoprotein. J. Biol. Chem. *278*, 52629–52640.

Alam, A., Kowal, J., Broude, E., Roninson, I., and Locher, K.P. (2019). Structural insight into substrate and inhibitor discrimination by human P-glycoprotein. Science *363*, 753–756.

Biasini, M., Bienert, S., Waterhouse, A., Arnold, K., Studer, G., Schmidt, T., Kiefer, F., Gallo Cassarino, T., Bertoni, M., Bordoli, L., et al. (2014). SWISS-MODEL: modelling protein tertiary and quaternary structure using evolutionary information. Nucleic Acids Res. *42*, W252–W258.

Brunner, J.D., Lim, N.K., Schenck, S., Duerst, A., and Dutzler, R. (2014). X-ray structure of a calcium-activated TMEM16 lipid scramblase. Nature *516*, 207–212.

Case, D.A., Cerutti, D.S., Cheatham, T.E., III, Darden, T.A., Duke, R.E., Giese, T.J., Gohlke, H., Götz, A.W., Greene, D.A., Homeyer, N., et al. (2017). AMBER 2017 (University of California).

Chen, P.-C., and Kuyucak, S. (2011). Accurate determination of the binding free energy for KcsA-charybdotoxin complex from the potential of mean force calculations with restraints. Biophys. J. *100*, 2466–2474.

Chovancova, E., Pavelka, A., Benes, P., Strnad, O., Brezovsky, J., Kozlikova, B., Gora, A., Sustr, V., Klvana, M., Medek, P., et al. (2012). Caver 3.0: a tool for the analysis of transport pathways in dynamic protein structures. PLoS Comp. Biol. *8*, e1002708.

Crespo, A., Martí, M.A., Estrin, D.A., and Roitberg, A.E. (2005). Multiple-steering QM-MM calculation of the free energy profile in chorismate mutase. J. Am. Chem. Soc. *127*, 6940–6941.

Darden, T.A., York, D.M., and Pedersen, L. (1993). Particle mesh Ewald - an N·Log(N) method for Ewald sums in large systems. J. Chem. Phys. *98*, 10089–10092.

Dickson, C.J., Madej, B.D., Skjevik, Å.A., Betz, R.M., Teigen, K., Gould, I.R., and Walker, R.C. (2014). Lipid14: the amber lipid force field. J. Chem. Theor. Comput. *10*, 865–879.

Duan, Z., Brakora, K.A., and Seiden, M.V. (2004). Inhibition of ABCB1 (MDR1) and ABCB4 (MDR3) expression by small interfering RNA and reversal of paclitaxel resistance in human ovarian cancer cells. Mol. Cancer Ther. *3*, 833–838.

Edelheit, O., Hanukoglu, A., and Hanukoglu, I. (2009). Simple and efficient site-directed mutagenesis using two single-primer reactions in parallel to generate mutants for protein structure-function studies. BMC Biotechnol. *9*, 61.

Ellinger, P., Kluth, M., Stindt, J., Smits, S.H.J., and Schmitt, L. (2013). Detergent screening and purification of the human liver ABC transporters BSEP (ABCB11) and MDR3 (ABCB4) expressed in the yeast Pichia pastoris. PLoS One *8*, e60620.

Epand, R.M., and Ruysschaert, J.-M. (2017). The Biophysics of Cell Membranes: Biological Consequences (Springer Berlin Heidelberg).

Feenstra, K.A., Pirovano, W., Krab, K., and Heringa, J. (2007). Sequence harmony: detecting functional specificity from alignments. Nucleic Acids Res. *35*, W495–W498.

Gowers, R.J., Linke, M., Barnoud, J., Reddy, T.J.E., Melo, M.N., Seyler, S.N., Domański, J., Dotson, D.L., Buchoux, S., Kenney, I.M., *et al.* (2016). MDAnalysis: A Python Package for the Rapid Analysis of Molecular Dynamics Simulations. Paper presented at: 15th Python in Science Conference (SciPy 2016) (Austin, Texas).

Grossfield, A. (2020). WHAM: An Implementation of the Weighted Histogram Analysis Method, Version 2.0.10.2. http://membrane.urmc.rochester.edu/?page_id=126.

Henikoff, S., and Henikoff, J.G. (1992). Amino acid substitution matrices from protein blocks. Proc. Natl. Acad. Sci. U S A *89*, 10915–10919.

Hollenstein, K., Dawson, R.J.P., and Locher, K.P. (2007). Structure and mechanism of ABC transporter proteins. Curr. Opin. Struct. Biol. *17*, 412–418.

Ishigami, M., Tominaga, Y., Nagao, K., Kimura, Y., Matsuo, M., Kioka, N., and Ueda, K. (2013). ATPase activity of nucleotide binding domains of human MDR3 in the context of MDR1. Biochim. Biophys. Acta *1831*, 683–690.

Jo, S., Kim, T., Iyer, V.G., and Im, W. (2008). CHARMM-GUI: a web-based graphical user interface for CHARMM. J. Comput. Chem. *29*, 1859–1865.

Jorgensen, W.L., Chandrasekhar, J., Madura, J.D., Impey, R.W., and Klein, M.L. (1983). Comparison of simple potential functions for simulating liquid water. J. Chem. Phys. *79*, 926–935.

Juliano, R.L., and Ling, V. (1976). A surface glycoprotein modulating drug permeability in Chinese hamster ovary cell mutants. Biochim. Biophys. Acta *455*, 152–162.

Kästner, J. (2011). Umbrella sampling. WIREs Comput. Mol. Sci. *1*, 932–942.

Kim, Y., and Chen, J. (2018). Molecular structure of human P-glycoprotein in the ATP-bound, outward-facing conformation. Science *359*, 915–919.

Kluth, M., Stindt, J., Dröge, C., Linnemann, D., Kubitz, R., and Schmitt, L. (2015). A mutation within the extended X loop abolished substrate-induced ATPase activity of the human liver ATP-binding cassette (ABC) transporter MDR3. J. Biol. Chem. *290*, 4896–4907.

Kornberg, R.D., and McConnell, H.M. (1971). Inside-outside transitions of phospholipids in vesicle membranes. Biochemistry *10*, 1111–1120.

Kroll, T., Prescher, M., Smits, S.H.J., and Schmitt, L. (2020). Structure and function of hepatobiliary ATP binding cassette transporters. Chem. Rev. *121*, 5240–5288.

Kumar, S., Rosenberg, J.M., Bouzida, D., Swendsen, R.H., and Kollman, P.A. (1992). The weighted histogram analysis method for free-energy calculations on biomolecules. I. The method. J. Comput. Chem. *13*, 1011–1021.

Le Grand, S., Götz, A.W., and Walker, R.C. (2013). SPFP: speed without compromise-A mixed precision model for GPU accelerated molecular dynamics simulations. Comput. Phys. Commun. *184*, 374–380.

Li, J., Jaimes, K.F., and Aller, S.G. (2014). Refined structures of mouse P-glycoprotein. Protein Sci. *23*, 34–46.

Litman, T., Zeuthen, T., Skovsgaard, T., and Stein, W.D. (1997). Structure-activity relationships of P-glycoprotein interacting drugs: kinetic characterization of their effects on ATPase activity. Biochim. Biophys. Acta *1361*, 159–168.

Lomize, M.A., Pogozheva, I.D., Joo, H., Mosberg, H.I., and Lomize, A.L. (2012). OPM database and PPM web server: resources for positioning of proteins in membranes. Nucleic Acids Res. *40*, D370–D376.

Maier, J.A., Martinez, C., Kasavajhala, K., Wickstrom, L., Hauser, K.E., and Simmerling, C.L. (2015). ff14SB: improving the accuracy of protein side chain and backbone parameters from ff99SB. J. Chem. Theor. Comput *11*, 3696–3713.

Manolaridis, I., Jackson, S.M., Taylor, N.M.I., Kowal, J., Stahlberg, H., and Locher, K.P. (2018). Cryo-EM structures of a human ABCG2 mutant trapped in ATP-bound and substrate-bound states. Nature *563*, 426–430.

Michaud-Agrawal, N., Denning, E.J., Woolf, T.B., and Beckstein, O. (2011). MDAnalysis: a toolkit for the analysis of molecular dynamics simulations. J. Comput. Chem. *32*, 2319–2327.

Nosol, K., Romane, K., Irobalieva, R.N., Alam, A., Kowal, J., Fujita, N., and Locher, K.P. (2020). Cryo-EM structures reveal distinct mechanisms of inhibition of the human multidrug transporter ABCB1. Proc. Natl. Acad. Sci. U S A *117*, 26245–26253.

Olsen, J.A., Alam, A., Kowal, J., Stieger, B., and Locher, K.P. (2020). Structure of the human lipid exporter ABCB4 in a lipid environment. Nat. Struct. Mol. Biol. *27*, 62–70.

Olsson, M.H.M., Søndergaard, C.R., Rostkowski, M., and Jensen, J.H. (2011). PROPKA3: consistent treatment of internal and surface residues in empirical pKa predictions. J. Chem. Theor. Comput *7*, 525–537.

Pastor, R.W., Brooks, B.R., and Szabo, A. (1988). An analysis of the accuracy of Langevin and molecular-dynamics algorithms. Mol. Phys. *65*, 1409–1419.

Pauli-Magnus, C., Mürdter, T., Godel, A., Mettang, T., Eichelbaum, M., Klotz, U., and Fromm, M.F. (2001). P-glycoprotein-mediated transport of digitoxin,

alpha-methyldigoxin and beta-acetyldigoxin. Naunyn-schmiedeberg's Arch. Pharmacol. *363*, 337–343.

Perez, C., Gerber, S., Boilevin, J., Bucher, M., Darbre, T., Aebi, M., Reymond, J.-L., and Locher, K.P. (2015). Structure and mechanism of an active lipid-linked oligosaccharide flippase. Nature *524*, 433–438.

Perez, C., Mehdipour, A.R., Hummer, G., and Locher, K.P. (2019). Structure of outward-facing PglK and molecular dynamics of lipid-linked oligosaccharide recognition and translocation. Structure *27*, 669–678 e665.

Pirovano, W., Feenstra, K.A., and Heringa, J. (2006). Sequence comparison by sequence harmony identifies subtype-specific functional sites. Nucleic Acids Res. *34*, 6540–6548.

Prescher, M., Smits, S.H.J., and Schmitt, L. (2020). Stimulation of ABCB4/MDR3 ATPase activity requires an intact phosphatidylcholine lipid. J. Lipid Res. *61*, 1605–1616.

Qian, H., Zhao, X., Cao, P., Lei, J., Yan, N., and Gong, X. (2017). Structure of the human lipid exporter ABCA1. Cell *169*, 1228–1239 e1210.

Roe, D.R., and Cheatham, T.E., III (2013). PTRAJ and CPPTRAJ: software for processing and analysis of molecular dynamics trajectory data. J. Chem. Theor. Comput *9*, 3084–3095.

Rosing, J., and Slater, E.C. (1972). The value of ΔG° for the hydrolysis of ATP. Biochim. Biophys. Acta *267*, 275–290.

Rostkowski, M., Olsson, M.H.M., Søndergaard, C.R., and Jensen, J.H. (2011). Graphical analysis of pH-dependent properties of proteins predicted using PROPKA. BMC Struct. Biol. *11*, 6.

Ruetz, S., and Gros, P. (1994). Phosphatidylcholine translocase: a physiological role for the mdr2 gene. Cell *77*, 1071–1081.

Ryckaert, J.-P., Ciccotti, G., and Berendsen, H.J.C. (1977). Numerical integration of the cartesian equations of motion of a system with constraints: molecular dynamics of n-alkanes. J. Comput. Phys. *23*, 327–341.

Salomon-Ferrer, R., Case, D.A., and Walker, R.C. (2013a). An overview of the Amber biomolecular simulation package. Wiley Interdiscip Rev Comput Mol Sci *3*, 198–210.

Salomon-Ferrer, R., Götz, A.W., Poole, D., Le Grand, S., and Walker, R.C. (2013b). Routine microsecond molecular dynamics simulations with AMBER on GPUs. 2. Explicit solvent particle mesh Ewald. J. Chem. Theor. Comput. *9*, 3878–3888.

Sapay, N., Bennett, W.F.D., and Tieleman, D.P. (2010). Molecular simulations of lipid flip-flop in the presence of model transmembrane helices. Biochemistry *49*, 7665–7673.

Sastry, G.M., Adzhigirey, M., Day, T., Annabhimoju, R., and Sherman, W. (2013). Protein and ligand preparation: parameters, protocols, and influence on virtual screening enrichments. J. Comput. Aid. Mol. Des. *27*, 221–234.

Sharom, F.J. (2014). Complex interplay between the P-glycoprotein multidrug efflux pump and the membrane: its role in modulating protein function. Front. Oncol. *4*, 41.

Shivakumar, D., Harder, E., Damm, W., Friesner, R.A., and Sherman, W. (2012). Improving the prediction of absolute solvation free energies using the next generation OPLS force field. J. Chem. Theor. Comput. *8*, 2553–2558.

Shivakumar, D., Williams, J., Wu, Y., Damm, W., Shelley, J.C., and Sherman, W. (2010). Prediction of absolute solvation free energies using molecular dynamics free energy perturbation and the OPLS force field. J. Chem. Theor. Comput. *6*, 1509–1519.

Shukla, S., Abel, B., Chufan, E.E., and Ambudkar, S.V. (2017). Effects of a detergent micelle environment on P-glycoprotein (ABCB1)-ligand interactions. J. Biol. Chem. *292*, 7066–7076.

Smit, J.J.M., Schinkel, A.H., Oude Elferink, R.P.J., Groen, A.K., Wagenaar, E., van Deemter, L., Mol, C.A.A.M., Ottenhoff, R., van der Lugt, N.M.T., van Roon, M.A., et al. (1993). Homozygous disruption of the murine mdr2 P-glycoprotein gene leads to a complete absence of phospholipid from bile and to liver disease. Cell *75*, 451–462.

Smith, A.J., van Helvoort, A., van Meer, G., Szabó, K., Welker, E., Szakács, G., Váradi, A., Sarkadi, B., and Borst, P. (2000). MDR3 P-glycoprotein, a phosphatidylcholine translocase, transports several cytotoxic drugs and directly interacts with drugs as judged by interference with nucleotide trapping. J. Biol. Chem. *275*, 23530–23539.

Souaille, M., and Roux, B. (2001). Extension to the weighted histogram analysis method: combining umbrella sampling with free energy calculations. Comput. Phys. Commun. *135*, 40–57.

Szöllősi, D., Chiba, P., Szakacs, G., and Stockner, T. (2020). Conversion of chemical to mechanical energy by the nucleotide binding domains of ABCB1. Sci. Rep. *10*, 2589.

Tieleman, D.P., and Marrink, S.-J. (2006). Lipids out of equilibrium: energetics of desorption and pore mediated flip-flop. J. Am. Chem. Soc. *128*, 12462–12467.

Torrie, G.M., and Valleau, J.P. (1977). Non-physical sampling distributions in monte-carlo free-energy estimation - umbrella sampling. J. Comput. Phys. *23*, 187–199.

van der Bliek, A.M., Baas, F., ten Houte de Lange, T., Kooiman, P.M., van der Velde-Koerts, T., and Borst, P. (1987). The human mdr3 gene encodes a novel P-glycoprotein homologue and gives rise to alternatively spliced mRNAs in liver. EMBO J. *6*, 3325–3331.

van der Bliek, A.M., Kooiman, P.M., Schneider, C., and Borst, P. (1988). Sequence of mdr3 cDNA encoding a human P-glycoprotein. Gene *71*, 401–411.

van Helvoort, A., Smith, A.J., Sprong, H., Fritzsche, I., Schinkel, A.H., Borst, P., and van Meer, G. (1996). MDR1 P-glycoprotein is a lipid translocase of broad specificity, while MDR3 P-glycoprotein specifically translocates phosphatidylcholine. Cell *87*, 507–517.

Waterhouse, A., Bertoni, M., Bienert, S., Studer, G., Tauriello, G., Gumienny, R., Heer, F.T., de Beer, T.A.P., Rempfer, C., Bordoli, L., et al. (2018). SWISS-MODEL: homology modelling of protein structures and complexes. Nucleic Acids Res. *46*, W296–W303.

Wu, E.L., Cheng, X., Jo, S., Rui, H., Song, K.C., Dávila-Contreras, E.M., Qi, Y., Lee, J., Monje-Galvan, V., Venable, R.M., et al. (2014). CHARMM-GUI Membrane Builder toward realistic biological membrane simulations. J. Comput. Chem. *35*, 1997–2004.

STAR★METHODS

KEY RESOURCE TABLE

REAGENT OR RESOURCE	SOURCE	IDENTIFIER
Antibodies		
α-C219 antibody from mouse	Merck	Cat# 517310
α-mouse antibody from goat	Jackson Immuno Research	Cat# 31-1292-ABO
Bacterial and virus strains		
XL1-blue Escherichia coli	(Ellinger et al., 2013)	N/A
Chemicals, peptides, and recombinant proteins		
Bodipy FL	Invitrogen	Cat# B10250
Fos-choline 16	Anatrace	Cat# F316S 25 GM
PK LDH	Merck	Cat# P0294-5ML
Deposited data		
Structure of inward-facing murine ABCB1	(Li et al., 2014)	PDB: 4M1M
Structure of outward-facing human ABCB1	(Kim and Chen, 2018)	PDB: 6C0V
Structure of outward-facing human ABCB4	(Olsen et al., 2020)	PDB: 6S7P
Experimental models: Organisms/strains		
X33 Pichia pastoris	(Ellinger et al., 2013)	N/A
Oligonucleotides		
Forward Primer for aa exchange Q52L in ABCB4 CGATACTCCGATTGGCTGGATAAATTGTTTATGT CGC	This paper	N/A
Forward Primer for aa exchange S58V in ABCB4 GGCTGGATAAATTGTTTATGGTTCTGGGT ACCATCATGGCCATAGC	This paper	N/A
Forward Primer for aa exchange S69A in ABCB4 GGCCATAGCTCACGGAGCTGGTCTCCCCCTCATG	This paper	N/A
Forward Primer for aa exchange Q52L, S58V in ABCB4 CGATACTCCGATTGGCTGGATAAATTGTTTATGGTTC	This paper	N/A
Recombinant DNA		
pSGP18_2μ_MDR3	(Ellinger et al., 2013)	N/A
Software and algorithms		
Prism 7	GraphPad	https://www.graphpad.com/scientific-software/prism/
Schrödinger Software Suite	Schrödinger, LLC, New York, NY, 2018	https://www.schrodinger.com/
SWISS-MODEL	(Biasini et al., 2014; Waterhouse et al., 2018)	https://swissmodel.expasy.org/
Amber17 Software Suite	(Case et al., 2017)	http://ambermd.org/
WHAM	(Grossfield, 2020; Kumar et al., 1992)	http://membrane.urmc.rochester.edu/content/wham/

RESOURCE AVAILABILITY

Lead contact

If further information are needed please contact the corresponding author Lutz.Schmitt@hhu.de.

Materials availability

The study did not generate new unique reagents. Chemicals were usually obtained from ThermoFisher (Germany) if not stated otherwise. All related material may also be contained by contacting the lead contact.

Data and code availability

All data are contained within the manuscript.

EXPERIMENTAL MODEL AND SUBJECT DETAILS

A pSGP18 plasmid backbone in which isoform two of the ABCB4 gene (databank NM_000443.3) was inserted was cloned into X33 *P. pastoris*. Typically *P. pastoris* was grown in baffled flaks at 30°C in MGY media (1.34 % yeast nitrogen base, 1 % glycerol, $4 \cdot 10^{-5}$ % Biotin) or for expression MM Medium (1.34 % yeast nitrogen base, 0.5 % methanol, $4 \cdot 10^{-5}$ % biotin) for 24 h or upscaled in a 7L fermentator in minimal glycerol medium (26.7 ml/l phosphoric acid; 0.93 g/l calcium sulfate; 18.2 g/l potassium sulfate; 14.9 g/l magnesium sulfate heptahydrate; 4.13 g/l potassium hydroxide; 40 g/l glycerol) and induced with methanol,

METHOD DETAILS

In vitro characterization of ABCB4 and its mutants

Cloning

The cloning procedures were described in detail in Ellinger et al., 2013 (Ellinger et al., 2013). Briefly, pSGP18 was cloned with a 2μ cloning site suitable for *S. cerevisiae*, *E. coli*, and X33 *P. pastoris* cultivation, in which isoform two of the ABCB4 gene (databank NM_000443.3) was inserted. At the C-terminus, nucleotides coding for a hexa-His-tag and a calmodulin affinity tag were added. Mutations were introduced by site-directed mutagenesis according to (Edelheit et al., 2009).

Transformation and test expression

Linearized (cut with MssI) pSGP18-2μ-ABCB4 plasmid was transformed in 80 μl competent X33 *Pichia pastoris* cells via electroporation with a 1500 V pulse for 5 ms. Cell recovery was performed with 1 ml YPD for 1 h at 30°C without shaking, followed by 2 h with shaking at 30°C and 210 rpm. Cells were stroke on selection agar plates with 100 – 1000 μg/ml zeocin. Expression tests were performed in 50 ml MGY media (1.34% yeast nitrogen base, 1% glycerol, $4 \cdot 10^{-5}$ % Biotin) in 200 ml baffled flasks for 24 h. Protein expression was induced with a media change to MM Medium (1.34 % yeast nitrogen base, 0.5 % methanol, $4 \cdot 10^{-5}$ % biotin) for 24 h. Crude membranes were prepared prior to Western blot analysis. *P. pastoris* clones with the highest ABCB4 protein expression were selected for fermentation as described in detail in (Ellinger et al., 2013).

Fermentation

Verified X33 *Pichia pastoris* cells carrying the pSGP18-2μ-ABCB4(-wt, -Q52L (L), -S58V (V), -S69A (A), -Q52L and S58V (LV), -Q52L, S58V, and S69A (LVA)) plasmid were grown on a YPD selection plate containing 200 mg/ml zeocin for 2 days. 1 l precultures were grown in 2 l baffled flasks for 18 h in MGY media and completely used for inoculation of a 6 l benchtop fermenter containing minimal glycerol medium (26.7 ml/l phosphoric acid; 0.93 g/l calcium sulfate; 18.2 g/l potassium sulfate; 14.9 g/l magnesium sulfate heptahydrate; 4.13 g/l potassium hydroxide; 40 g/l glycerol). After the batch glycerol was consumed, cells were fed by glycerol for 5 h to increase biomass. Protein induction was accomplished by a methanol feed for 24 h. After harvesting, cells were washed with 50 mM Tris-HCl pH 8.0 and re-pelleted. Cell masses reaching 1.3±0.2 kg were obtained for all *Pichia pastoris* cells expressing the ABCB4 mutants. These were aliquoted (100 g batches), flash-frozen in liquid nitrogen, and stored at -80 °C until further use.

Preparation of crude membrane vesicles

All purification steps were conducted at 4 °C. Usually, 100 g frozen cells were thawed on ice, and crude membranes were prepared. Therefore, cells were resuspended in lysis buffer (0.33 M sucrose; 100 mM 6-aminohexanoic acid; 1 mM EGTA; 1 mM EDTA; 50 mM Tris-HCl pH 8.0; NaCl) in a 1:5 ratio. Cells were disrupted at 2.7 kbar with a cell disruptor system (I&L constant systems). Differential centrifugal steps separated cell debris from crude membrane vesicles. Crude membrane vesicles were collected at 138000 x *g* and resuspended in membrane buffer (50 mM Tris-HCl pH 8.0; 150 mM NaCl, 30 % (v/v) glycerol, protease inhibitor cocktail (Roche)). Total protein concentration was determined with a Bradford assay following the standard protocol (Roche).

Solubilization

Crude membrane vesicles were diluted to 10 mg/ml total protein concentration and supplemented with 1 % (w/v) Fos-Choline-16 (FC-16, Anatrace). Protein solubilization was performed for 1 h at 18 °C. Non-solubilized parts were removed at 138000 x *g* for 1 h.

Tandem affinity purification

20 mM imidazole was added to the solubilized membranes to increase binding selectivity. The solution was loaded on a 5 ml HiTrap chelating column (GE healthcare) loaded with Ni^{2+} ions, washed with washing buffer (50 mM Tris-HCl pH 8.0; 50 mM NaCl; 30 % glycerin (v/v); 0.0011 % (w/v) FC-16; 20 mM imidazole) to baseline level and eluted in one step with elution buffer (50 mM Tris-HCl pH 8.0; 50 mM NaCl; 30 % (v/v) glycerin; 0.0011 % (w/v) FC-16; 200 mM imidazole). Fractions of the immobilized metal ion affinity chromatography (IMAC) with the highest absorbance at 280 nm were pooled and transferred onto a calmodulin affinity resin (GE Healthcare) and incubated overnight with gentle rotation at 4 °C. Calmodulin affinity purification (CAC) was conducted according to a standard protocol (GE healthcare). Aliquots with the highest protein concentration were pooled and either directly used for ATPase activity measurements or flash-frozen in liquid nitrogen and stored at –80 °C until further use. Yields were quantified via NanoDrop measurements and were for all ABCB4 mutants including the ABCB4 wildtype around 5 ± 1.7 μg per purification out of 100 g wet cell mass.

Compound preparation

Lipids were purchased from Avanti Polar Lipids and resuspended in chloroform. Chloroform was removed in a vacuum oven at 40 °C by stepwise increasing the applied vacuum. After 30 min at the lowest pressure levels, lipids were hydrated in suspension buffer (50 mM Tris-HCl pH 8.0; 150 mM NaCl). A sonication step for 5– 10 min was included to decrease the turbidity of the solution. Dilution series for ATPase measurements were prepared with suspension buffer.

Digitoxin was dissolved in DMSO, verapamil in ethanol. The amount of solvent used in the actual ATPase reaction did not exceed 5 %, and background measurements were performed in the presence of the same volume of solvent.

Enzyme coupled ATPase assay

The ATPase activity of detergent purified ABCB4 was determined by an enzyme coupled assay (Prescher et al., 2020). Briefly, a standard ATPase reaction volume was 200 µl in total composed of 50 mM Tris-HCl pH 7.4 at 37 °C; 5 mM $MgCl_2$; 4 mM phosphoenolpyruvate; 0.6 mM NADH (reduced); 13 units pyruvate kinase (PK); 16 units lactate dehydrogenase (LDH); 0.0011 % (w/v) FC-16 and 35 µg/ml (239 nM) detergent purified protein. Substrate stock solutions were compounded, and 5 or 10 µl solution was added to the ATPase reactions keeping the solvent concentration below 5 % (v/v). The reaction was started by the addition of 5 mM ATP. The absorbance of NADH was followed for 60 min. Since the NADH oxidation is stoichiometric to ATP hydrolysis, the ATPase activity of ABCB4 could be expressed as nmol ATP consumption per mg of ABCB4 protein and minute. A background measurement was always subtracted from the data points. Here, the cysteine residue in the Walker A motive of ABCB4 was labeled with the fluorophore FL-maleimide-bodipy and was conducted in a separate reaction (Kluth et al., 2015). The steric constraints imposed by the fluorophore prevent ATPase activity of ABCB4. No influences on the PK or LDH performance due to compound or solvent concentrations were observed.

Molecular modeling and simulations

Comparative modeling of inward-facing ABCB1 and ABCB4 for molecular dynamics simulations

Comparative models of inward-facing human ABCB1 (UniProt ID: P08183) and ABCB4 (UniProt ID: P21439) were generated in BioLuminate® (Schrödinger Release 2018-1: BioLuminate, Schrödinger, LLC, New York, NY, 2018) using the structure of inward-facing murine P-glycoprotein (PDB ID: 4M1M, (Li et al., 2014)) as a template. Target-template sequence alignments (Figure S7A) were extracted from a multiple sequence alignment of *H. sapiens* ABCB1, ABCB4, ABCB5, ABCB11, *M. musculus* ABCB1A/B, ABCB4, ABCB5, ABCB11, *R. norvegicus* ABCB1, ABCB4, ABCB11, *C. griseus* ABCB1, PGY2, ABCB4, *O. cuniculus* ABCB11, and the sequence of the template structure deposited in the PDB, corrected for the crystallographically resolved aa. Loops with more than ten missing residues in the template structure were not modeled in the target structure; shorter loops were modeled with Prime (Schrödinger Release 2018-1: Prime, Schrödinger, LLC, New York, NY, 2018). The resulting models were subjected to the Protein Preparation Wizard (Schrödinger Release 2018-1: Protein Preparation Wizard; Epik, Schrödinger, LLC, New York, NY, 2018, (Sastry et al., 2013)): N- and C-terminal residues were capped with ACE and NMA residues, respectively. The PROPKA (Olsson et al., 2011; Rostkowski et al., 2011) implementation in the Schrödinger Suite was used to calculate aa protonation states at pH 7.0. Neutral glutamate, asparate, and lysine residues were reverted to their charged state. For histidines, the calculated HID/HIE/HIP states were kept as calculated. Subsequently, both structures were minimized to a maximum RMSD value of 0.3 Å and analyzed using the Protein Reliability module in the Schrödinger Suite. Residues with large deviations from the allowed backbone and side chain dihedreals were minimized with Prime using the VSGB solvation model (Shivakumar et al., 2010, 2012) and an implicit membrane placed according to the entry of the template structure in the OPM database (Lomize et al., 2012).

Comparative modeling of outward-facing ABCB4 for potential of mean force calculations

An initial model of outward-closed human ABCB4 (UniProt ID: P21439) was generated with the SWISS-MODEL server (Biasini et al., 2014; Waterhouse et al., 2018) using the structure of ATP-bound ABCB1 as a template structure (PDB ID: 6C0V, (Kim and Chen, 2018)). Model refinement was performed according to the procedure outlined in section 11.5.2. At the time of model creation, the cryo-EM structure of ABCB4 (PDB ID: 6S7P, (Olsen et al., 2020)) was not yet available. However, a C-alpha RMSD of < 1.0 Å between the cryo-EM structure (resolution: 3.20 Å) and our model (Figure S7B) indicated very good model accuracy.

Molecular dynamics simulations of inward-facing ABCB1 and ABCB4

To study the conformational dynamics of ABCB1 and ABCB4, and to assess whether and to what extent the two ABC transporters are capable of binding DOPC lipids, we conducted five independent all-atom MD simulations of each inward-facing transporter model (cf. section 11.5.2) embedded in an explicit DOPC bilayer. The orientation of ABCB1 and ABCB4 in the membrane was adopted from the orientation of the respective template structure (cf. section 11.5.2) in the OPM database (Lomize et al., 2012) and was then used to embed the simulation system into an explicit DOPC lipid bilayer using using the CHARMM-GUI (Jo et al., 2008) Membrane/Bilayer Builder (Wu et al., 2014) (water layer thickness: 20 Å, rectangular box, 0.154 M NaCl ions placed using the Monte Carlo algorithm). Topology files were built using the tLEaP module in AmberTools 17 (Case et al., 2017). The AMBER ff14SB force field (Maier et al., 2015) was used to describe the protein and the AMBER Lipid14 force field (Dickson et al., 2014) to describe the DOPC lipids. Water molecules were described with the TIP3P water model (Jorgensen et al., 1983).

MD Simulations were carried out using the mixed-precision SPFP GPU implementation of pmemd (Le Grand et al., 2013; Salomon-Ferrer et al., 2013b) implemented in the Amber17 Suite of biomolecular simulation programs (Case et al., 2017; Salomon-Ferrer et al., 2013a). A time step of 2 fs was used for integration, and the Langevin thermostat (Pastor et al., 1988) was used for temperature control with a collision frequency of $\gamma = 1\ ps^{-1}$ and a target temperature of $T = 300$ K. Covalent bonds between heavy atoms and hydrogen atoms were constrained using the SHAKE algorithm (Ryckaert et al., 1977). The Particle Mesh Ewald method (Darden et al., 1993)

was used to estimate long-range electrostatic interactions; the cutoff for short-range electrostatics and van der Waals forces was set to 10 Å. Each simulation system was minimized and equilibrated five times independently according to the protocol outlined in Table S1.

Subsequently, for each of the two systems, 5×200 ns of NPT-MD was conducted, resulting in a cumulative simulation time of 2.0 μs. Coordinates were stored in time steps of 20 ps. Post-processing and analysis of the MD trajectories was carried out in CPPTRAJ (Roe and Cheatham, 2013) and the MDAnalysis python library (Gowers et al., 2016; Michaud-Agrawal et al., 2011). The integrity of the systems was verified via the root-mean-square deviation of the C-alpha positions and the density profile of the membrane components along the Z-axis (Figure S7B).

Generation of DOPC flip-flop pathways

First, to sample a pathway for a spontaneous flip-flop of a single DOPC molecule, a bilayer consisting of 100 DOPC molecules was generated using the CHARMM-GUI (Jo et al., 2008) Membrane/Bilayer Builder (Wu et al., 2014). Next, the coordinates of the central DOPC molecule were translated using tLEaP to construct a set of 44 systems in which the phosphorus atom of the phosphocholine moiety is progressively advanced by 1 Å along the Z-coordinate, starting from the center of the bilayer. All systems were minimized and equilibrated following the protocol used for the conventional MD simulations of ABCB1 and ABCB4 (cf. section 11.5.4 and Table S1 1), with only the harmonic restraints adjusted such that the distance between the Z-coordinates of the phosphorus atom of the translated DOPC molecule and the center of mass of the phosphorus atoms in the opposite leaflet was kept near the value of the input structure with a force constant of 4.0 kcal mol^{-1} $Å^{-2}$.

In contrast, the pathways for DOPC flop along TMH1 and TMH7 of inward-facing ABCB4 were not generated by hand, but were presampled via the steered MD (sMD) implementation in Amber17 (Crespo et al., 2005) to allow for minor lateral translations of the lipid whenever favorable interactions with the protein are within reach. The closest-to-average structures of the ABCB1 and ABCB4 MD simulations described in section 11.5.4 served as input coordinates for the sMD runs. A moving harmonic restraint with a force constant of 3.0 kcal mol^{-1} $Å^{-2}$ was employed, first, to reduce the distance between the Z-coordinates of the phosphorus atom of the DOPC molecule closest to the base of TMH1 or TMH7 and the center of mass of the phosphorus atoms in the upper leaflet.

The pathway for DOPC flop along TMH1 of outward-closed ABCB4 was generated accordingly. Here, the closest-to-average structure of an unbiased ABCB4/DOPC MD simulation served as input coordinates for the sMD run.

Potential of mean force calculations

Free-energy profiles for spontaneous DOPC flip-flop and DOPC flop along TMH1 and TMH7 of ABCB4 were computed from umbrella sampling MD simulations (Kästner, 2011; Torrie and Valleau, 1977) along the pregenerated pathways (cf. section 11.5.5) using the Weighted Histogram Analysis Method (WHAM) (Kumar et al., 1992; Souaille and Roux, 2001) as implemented by Alan Grossfield (Grossfield, 2020). The umbrella sampling simulations for spontaneous DOPC flip-flop were carried out using two sets of simulations. First, the 44 umbrella sampling windows (cf. section 11.5.5) were each sampled three times for 20 ns with the same restraint as used in the equilibration, except that the restraint force was reduced to 3.0 kcal mol^{-1} $Å^{-2}$. Then, in the second set of simulations (20 ns per window), the restraint force in each window was adjusted to match the energy at that window's position in a potential of mean force (PMF) calculated based on the first set of simulations. To calculate the final free energy profile, data from all windows (total simulation time: 3.52 μs) was pooled and analyzed with WHAM using 300 bins and a tolerance of 10^{-7}.

Free-energy profiles for DOPC flop along TMH1 and TMH7 of inward-facing ABCB4 were computed similarly. Starting structures for the umbrella sampling windows were extracted from the sMD run (cf. section 11.5.5) such that the flop coordinate was divided into 100 evenly spaced windows. Each window was sampled for 5 ns with a restraint force of 20.0 kcal mol^{-1} $Å^{-2}$ before an initial PMF was calculated with WHAM (300 bins, tolerance: 10^{-7}), which served as a guide for estimating the force constants for each window in the second set of simulations. This process was repeated two more times, resulting in simulation times of 20 ns per window and a total simulation time of 2 μs. The final free energy profile was calculated based on the pooled data from all windows.

Similarly, free-energy profiles for DOPC flop along TMH1 and TMH7 of outward-closed ABCB4 were computed using a single set of umbrella sampling simulations consisting of 80 windows of 50 ns length each (total simulation time: 4 μs). Starting structures were extracted from the sMD run (cf. section 11.5.4), and the force constants for each window were set to 20.0 kcal mol^{-1} $Å^{-2}$.

To calculate the degree of overlap between adjacent windows, we determined the mean and standard deviation within each window and calculated the intersecting area of the two corresponding normal distributions by numerical integration using Simpson's rule. The average degree of overlap was 62.7 ± 2.3 % (DOPC), 27.1 ± 0.8 % (IF), and 5.6 ± 0.1 % (OF), and, hence, well above or in line with values regarded as suitable for PMF calculations (Chen and Kuyucak, 2011). For each set of umbrella windows, we estimated the uncertainty in the PMF by dividing the data into five equally sized parts, calculating a PMF for each, and determining standard deviation and standard error of the mean of these five free energy profiles. The convergence of the free energy profiles for spontaneous DOPC flip-flop and ABCB4-assisted DOPC translocation is shown in Figure S7B.

Single-point free energy calculations on ABCB4 and ABCB1 hybrid mutations

Single-point free energy calculations on ABCB4 (V985M, H989Q, A990V, and combinations thereof) and ABCB1 hybrid mutations (M986V, Q990H, V991A, and combinations thereof) were performed using the Residue Scanning module in BioLuminate® (Schrödinger Release 2020-1: BioLuminate, Schrödinger, LLC, New York, NY, 2020) with four different settings: i) the protein structure was not preminimized and no implicit membrane was present during the stability calculations ("no minimization / no membrane); ii) the complete protein structure was preminimized in an implicit membrane environment with Prime (Schrödinger Release 2020-1: Prime, Schrödinger, LLC, New York, NY, 2020), but no implicit membrane was present during the stability calculations ("minimization / no membrane"); iii) the protein structure was not preminimized and an implicit membrane was present during the stability

calculations (“no minimization / implicit membrane”); iv) the complete protein structure was preminimized in an implicit membrane environment with Prime and an implicit membrane was also present during the stability calculations (“minimization / implicit membrane”). In either case, side-chain prediction with backbone minimization for residues within 8 Å of the mutation site was enabled.

QUANTIFICATION AND STATISTICAL ANALYSIS

ABCB4 and ABCB1 orthologs

ABCB4 and ABCB1 orthologs were searched on 18.1.21 at NCBI (https://www.ncbi.nlm.nih.gov/gene).

Calculation of the ATPase activity

For analysis, the background activity of ABCB4 labeled with bodipy (ABCB4-Bodipy) was subtracted. Kinetic parameters were analyzed using Prism 7 (GraphPad) and plotted either by Michaelis Menten kinetics (Equation 1), Litman (Equation 2) (Litman et al., 1997) or a dose-response fit (Equation 3). Here, $V_{(S)}$ represents the ATPase activity at a given compound concentration. V_0 is the basal ATPase activity without any compound, V_1 is the maximal ATPase activity, at which no inhibition occurred. V_2 corresponds to the activity at an infinite concentration of a compound, S the compound concentration, K_1 the compound concentration at half-maximal stimulating ATPase activity (at half V_1), and K_2 the compound concentration at half-maximal inhibitory concentration. B represents the plateau of the lowest ATPase activity, T the plateau of the highest ATPase activity, and H_S the Hill slope.

$$V_{(S)} = \frac{V_1 \cdot S}{K_1 + S} + V_0 \qquad \text{Michaelis} - \text{Menten equation} \qquad \text{(Equation 1)}$$

$$V_{(S)} = \frac{K_1 K_2 V_0 + K_2 V_1 S + V_2 S^2}{K_1 K_2 + K_2 S + S^2} \qquad \text{Litman equation} \qquad \text{(Equation 2)}$$

$$V_{(S)} = B + \frac{T - B}{1 + 10^{([\log(K_2)] - S) \cdot H_S)}} \qquad \text{Dose} - \text{response equation} \qquad \text{(Equation 3)}$$

The translocation rate of DOPC was calculated based on the assumption that two ATP molecules are hydrolyzed to translocate one DOPC molecule. Since the maximal velocity of DOPC-stimulated ATPase activity of ABCB4 wt is 149.7 ± 28 nmol ATP per min and mg isolated protein, a DOPC translocation rate of 658 ± 123 per hour results (molecular weight of 146,500 g mol^{-1}, ABCB4 wt and affinity tags). The Eyring equation was used to calculate theoretical barrier heights E from experimentally determined flip-flop or translocation rates k.

$$k = \frac{k_B T}{h} e^{-\frac{E}{RT}} \qquad \text{Eyring equation} \qquad \text{(Equation 4)}$$

Here k_B represents the Boltzmann constant, T the absolute temperature, h the Planck constant, and R the gas constant.